# Reverberation: Learning the Latencies Before Forecasting Trajectories

Conghao Wong, Ziqian Zou, Beihao Xia, and Xinge You, Senior Member, IEEE

Abstract—Bridging the past to the future, connecting agents both spatially and temporally, lies at the core of the trajectory prediction task. Despite great efforts, it remains challenging to explicitly learn and predict latencies, the temporal delays with which agents respond to different trajectory-changing events and adjust their future paths, whether on their own or interactively. Different agents may exhibit distinct latency preferences for noticing, processing, and reacting to any specific trajectorychanging event. The lack of consideration of such latencies may undermine the causal continuity of the forecasting system and also lead to implausible or unintended trajectories. Inspired by the reverberation curves in acoustics, we propose a new reverberation transform and the corresponding Reverberation (short for Rev) trajectory prediction model, which simulates and predicts different latency preferences of each agent as well as their stochasticity by using two explicit and learnable reverberation kernels, allowing for the controllable trajectory prediction based on these forecasted latencies. Experiments on multiple datasets, whether pedestrians or vehicles, demonstrate that Rev achieves competitive accuracy while revealing interpretable latency dynamics across agents and scenarios. Qualitative analyses further verify the properties of the proposed reverberation transform, highlighting its potential as a general latency modeling approach.

# I. INTRODUCTION

To live is to imagine ourselves in the future, and there we inevitably arrive. Human cognition and planning fundamentally rely on anticipating future outcomes from past experiences. Similarly, trajectory prediction seeks to forecast future positions for all agents based on their observed temporal patterns and potential interactions [1]. It can be used and applied in various intelligent systems and applications, including but not limited to behavior analyses [2]–[4], transportation systems [5]–[7], multi-agent decision systems [8]–[10], thus attracting increasing attention from more and more researchers.

As one of the time-series forecasting tasks, the modeling of temporal dependencies and relationships [11], [12] between every observation and prediction step has been widely researched in the field of trajectory prediction. Especially, this task is mostly *human-centric* in most of its application scenarios, making the discussions about such temporal steps even more philosophical. Prior researchers tried to capture temporal dependencies within trajectories using recurrent networks like RNNs [13] and LSTMs [1], [14], discussing how the next step

This work was supported by the National Natural Science Foundation of China under Grant 62172177.

Conghao Wong, Ziqian Zou, Beihao Xia, and Xinge You are with Huazhong University of Science and Technology, Wuhan 430074, Hubei, China (Email: conghaowong@icloud.com, ziqianzoulive@icloud.com, xbh\_hust@hust.edu.cn, youxg@mail.hust.edu.cn).

Code is available at https://github.com/cocoon2wong/Rev.

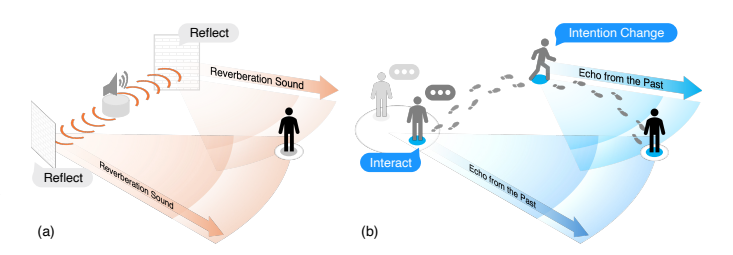


Fig. 1. Motivation illustration. Inspired by the acoustic reverberation that describes how the echo sound decays in the space after reflecting, we model how past trajectory-changing events (like intention changes or interactions) change trajectories as well as their latencies as "echoes from the past".

would be determined by the current state of an agent. Further, advanced neural networks like Transformers [15], [16], diffusion models [17], [18], and even knowledge transferred from large language models [19] have been introduced to this task to further explore how to bridge past observations to the future, not only simply from the time domain but additionally considering the spectral properties [20], [21] of trajectories.

Despite great efforts have been made, directly instructing neural networks to analyze and identify potential trajectorychanging events within observed trajectories and to predict the impact of these events at some specific future steps remains a challenging problem. For example, these methods might be hard to answer questions such as how long it takes for an event to begin affecting the trajectory, how long such an effect persists, and when its influence will dissipate. However, for the agents we concerned, whether pedestrians, vehicles, or robots, this is quite intuitive, like we always subconsciously calculate these intervals: how long after an event (whether self-sourced or socially interactive) occurs before it will be noticed by us, how long we wait before initiating a response and altering our trajectory, and finally how long it takes for us to finish these events. While current methods can bridge the past and the future to some extent, like capturing interactions or intention changes then making the corresponding trajectory modifications when forecasting, the span and precise location of these "bridges" remain unknown. This prevents the predictions from fully aligning with human intuition, leading to unexpected outcomes and diminished interpretability. Therefore, how to model and predict these unique temporal intervals, or simply we call latencies, when predicting trajectories, then guiding the prediction networks with such forecasted latencies, becomes our main concern in this manuscript.

Though the future is a product of every present that precedes it, tomorrow does not belong to today. As we described above, building bridges from the past to the future is a centerpiece

of the trajectory prediction task, but it remains challenging to clearly locate these bridges, as well as the potentially implicit latencies. The first problem we have to address is that the past and the future are not equivalent because of the causality [22], [23] of the system, where only events occurring in past can affect the future, and this effect is accompanied by a specific latency. Similar to our intuitive experience, the future (tomorrow) is a product of the past (present), but the process of such a product has specific temporal properties, or more accurately, specific time-frequency responses.

In the field of signal processing, the Fourier transform and its variations provide us with reference ideas for describing such time-frequency properties. Just as the Fourier transform decomposes a signal into the superposition of a number of sinusoids and analyzes its spectral properties by different superposition coefficients, a natural thought is that we can decompose a future trajectory, or at least its representation, into the superposition of the representations of past events, and to simulate latencies within trajectories by the corresponding superposition coefficients. Specifically, these superposition coefficients will be made trainable, thus further unlocking the potential of advanced neural networks for learning and simulating latencies in these trajectories in different scenarios. As with reverberation in acoustics (illustrated in Fig. 1 (a)), which describes the intensity decay of a sound wave as it is reflected and reaches a specific destination, we describe future trajectories as superimpositions of "echo ripples" from the past (Fig. 1 (b)), thus directly modeling the latencies for agents that respond to different trajectory-changing events. We call this transform the Reverberation Transform, which explicitly represents the latencies within the trajectory to respond to different trajectory-changing events at any past moment, and combines the representation of future trajectories as a shifted superposition of such past representations.

Specifically, similar to the matrix form of the Fourier transform, we use two coefficient matrices, called reverberation kernels, to further decompose and inscribe latencies for handling trajectory-changing events. Both kernels will be made trainable and are unique for each ego agent. Denote the observation and the prediction length as  $T_h$  and  $T_f$ , to better capture and highlight the differences between different trajectory-changing events during the observation period, this transform will actually act on the similarity matrix of the encoded sequential feature, where each of whose feature dimension will be expanded in to a matrix of  $T_h \times T_h$ . Then, this similarity matrix will be right-multiplied by a Reverberation Kernel  $\mathbf{R} \in \mathbb{R}^{T_h \times T_f}$  that serves as the baseline of latency-coefficients, thus decomposing future trajectories on all  $T_f$  steps as a combination of  $T_h$  observed features. Then, given agents' diversities and stochasticities, we regard that there are also stochasticities in their latency preferences. Thus, similar to previous multi-style approaches [6], the above representation will be further left-multiplied by a Generating Kernel  $\mathbf{G}^{ op} \in \mathbb{R}^{K_g \times T_h}$  with  $K_g$  generating channels to simultaneously obtain forecastings  $(K_g \times T_f)$  for each feature dimension) with different latency-preferences. With the proposed reverberation transform, each agent's unique latency preference will be predicted by these two kernels, thus explicitly enabling the prediction of latencies for different trajectory-changing events, and further using these latencies as a priori to enable interpretable trajectory forecasting.

In summary, our main contributions are as follows:

- We propose the reverberation transform to explicitly model agents' latencies in handling trajectory-changing events, consisting of two trainable reverberation kernels: the reverberation kernel R that models event-level causal latencies and the generating kernel G that simulates variations and alternatives of such latencies.
- We design the Reverberation (short for Rev) trajectory prediction model, which builds upon the proposed reverberation transform, to simultaneously learn non-interactive and social latencies, thereby enabling latency-aware and interpretable trajectory prediction.
- We validate the proposed Rev both quantitatively and qualitatively on multiple trajectory datasets, and extensively analyze the theoretical properties of the proposed reverberation transform. Extensive ablations and discussions further verify both the quantitative improvements and the interpretability of the learned latency dynamics.

#### II. RELATED WORKS

#### A. Trajectory Prediction and Social Interactions

Trajectory prediction aims at predicting agents' future movements based on their observed states and interactions with others [1]. Researchers have increasingly focused attention on the modeling of social interactions when forecasting. Early works use handcrafted or physical rules to simulate the interacting forces between agents or environments. Social Force [24] regards pedestrian motion as a system of attractive and repulsive forces, while the velocity obstacle [25] and reciprocal velocity obstacle [26] frameworks model collision avoidance via geometric velocity constraints. With the development of data-based methods, sequential models like RNNs [27], [28] and LSTMs [1], [29], [30] are then introduced to capture implicit dynamic interactions among agents. Social-LSTM [1] first uses social pooling layer to model the target agent's local interactions with its surroundings, inspiring diverse follow-up works [10], [12], [31] with the same social-interaction-modeling fashion. Researchers further leverage attention mechanisms [32], [33] or Transformers [16], [34], [35], as well as structured information in GNNs [36]–[39], to globally capture complex interactions and group behaviors among agents.

Although countless great ideas or works have been proposed, it is still difficult for current approaches to cover all potential connections or interactions between intelligent agents, especially in more and more complex scenarios. Some researchers have recently introduced more interpretable theories to simulate such interactions from a more human-centric point of view. Inspired by echolocation of marine animals, Wong *et al.* [40], [41] use angle-based representation to model social interactions with surroundings by considering their velocity, distance and direction. Further, considering the knowledge embedded within language models and their potentials for drawing interactions, Bae *et al.* [42], [43] introduce large

language models with specially designed numeric tokens to reveal the spatial interactions from a brand new view. Emulating the resonance phenomenon, the *Resonance* [21] views social interactions as the co-vibrations of agents' spectrums, thus decomposing and interpreting randomness among agents when interacting. GPCC model [44] also takes the group preferences of pedestrians into account, using the long-term-distance kernel function to capture group interactions with a multi-level strategy. Despite their remarkable efforts, most current models neglect the consideration of latencies for noticing, handling, or finally terminating any specific social events over the trajectory-decision process, leading to the underestimation of interactions temporally.

# B. Temporal Dependencies and Latencies in Trajectories

Except for the social interactions, temporal dependencies in trajectories have been widely studied in the field of trajectory prediction. Researchers try to capture these dependencies through diverse theoretical approaches to deep neural networks, from the classic Social Force [24] to recurrent structures like RNNs [13], [27], [28], [45] or LSTMs [1], [46]–[48], or further attention-based networks like Transformers [7], [15], [49]–[51], and more recently, diffusion models [17], [52]–[55] and knowledge transferred from large language models [42], [43].

These models could effectively bridge agents' representations from the observation period to the prediction period, yet they lack explicit mechanisms to model potential temporal latencies. For example, each pedestrian may present different latency preferences for starting to notice something, start processing an event, and start modifying their trajectories. Note that this latency is not exactly equivalent to time dependence. Temporal dependence indicates how future representations will be represented through the current moment, whereas latency indicates how long after an interval the effects of a particular event will be apparent. Unfortunately, most of these current methods cannot predict this latency relationship.

Although our considered latencies, or more widely the temporal delays, have already been studied in the field of signal processing and control systems, such as delay compensation [56], [57], they are rarely considered or further treated as learnable variables in the trajectory prediction task. Human behavioral studies [58], [59] also reveal diverse reaction times, *i.e.*, diverse latency preferences, yet existing forecasting architectures cannot adaptively capture or predict such heterogeneous latencies across agents, not to mention their interactive behaviors. By trying to introduce the new reverberation transform, the proposed *Rev* model explicitly introduces learnable latency controls, thus extending the considerations of current trajectory prediction.

In summary, existing trajectory prediction models focus more on the modeling of spatial interactions or implicit temporal dependencies, without explicitly modeling when and how long past events influence agents' future motions. Prior temporal models are better at capturing sequential dependencies within trajectories but not latencies for agents to plan their

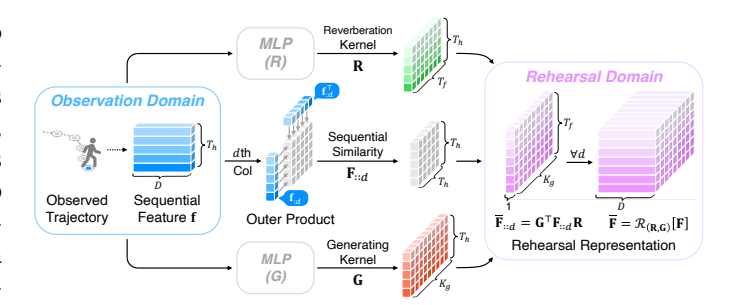


Fig. 2. Computation pipelines of the proposed reverberation transform. It aims at learning two reverberation kernels  ${\bf R}$  and  ${\bf G}$ , thus mapping sequential feature  ${\bf f}$  from the observation domain into the imagined rehearsal domain.

trajectories. Our work differs by explicitly formulating and learning latencies as trainable temporal responses, implemented through the proposed Reverberation Transform and the *Rev* trajectory prediction model, making it possible to take into account latencies while forecasting trajectories.

#### III. METHOD

In this section, we first formalize our considered trajectory prediction task, then introduce the proposed reverberation transform and the corresponding *Reverberation* (short for *Rev*) trajectory prediction model in detail.

#### A. Reverberation Transform

The foundation of the proposed *Rev* model is the reverberation transform. Like the acoustic reverberation curves, it is designed to describe how agents would instinctively modify their trajectory plans in anticipation of the upcoming prediction period, according to the trajectory-changing events they saw or have already experienced during observation. Here, the reverberation time indicates how long the ego agent will notice a trajectory-changing event and start to modify its own trajectory plan, as well as how long such modification will last or vanish in the future. These times could be all considered as the **latencies** to handle existing or possible trajectory-changing events for changing their own trajectory-plans, depending on their unique behavioral preferences.

The main focus of reverberation transform is to learn and forecast such latencies when agents plan their trajectories. Intuitively, people tend to imagine those upcoming events in their minds before they actually happen, as if they were doing a *dress rehearsal* before the live show. These trajectory plans are hypothesized and may not exactly be the same as their real future paths. Thus, as shown in Fig. 2, this transform aims at connecting ego agents' observations (the *observation* domain) and their immediate planning of future trajectories (the *rehearsal* domain), reflecting the instinctive latency of how ego agents respond to different trajectory determinants.

1) Sequential Similarity: Given the representation  $\mathbf{f} \in \mathbb{R}^{T_h \times D}$  of an observed sequential input (on  $T_h$  past steps, D is the feature dimension), we first construct the sequence-wise similarity  $\mathbf{F} = \sigma(\mathbf{f}) \in \mathbb{R}^{T_h \times T_h \times D}$  to characterize differences

4

of each temporal step within such representation. For the dth feature dimension (d = 1, 2, ..., D), we have its slice

$$\mathbf{F}_{::d} = \mathbf{f}_{:d} \mathbf{f}_{:d}^{\top}. \tag{1}$$

This helps emphasize the differences among temporal steps within the sequence, thereby highlighting salient observations or distinctive trajectory-changing events, making the following operations concentrate on the most unique step or event rather than the uniform feature patterns when modeling latencies.

2) Reverberation Kernels: The reverberation transform considers trajectories from two perspectives: the latencies of agents in handling trajectory determinants or modifying trajectories, and the randomness or variations within such latencies. Its basic thought is that agents' future plans could be uniquely represented by the linear combinations of their historical states. Especially, we regard that latencies for handling trajectory-changing events could be also represented by such kernels explicitly rather than indirectly, just like Fourier transforms decompose signals as direct combinations of sinusoids.

For each agent, this combination depends on a trainable *Reverberation Kernel*  $\mathbf{R} \in \mathbb{R}^{T_h \times T_f}$  and a trainable *Generating Kernel*  $\mathbf{G} \in \mathbb{R}^{T_h \times K_g}$ . We collectively refer to them as *Reverberation Kernels*. Elements in both reverberation kernels are limited to the range of [-1,1] via the tanh activation, limiting the range of transformed features while forcing the network to learn and distinguish these two kernels from their unique structures rather than the massive data-fitting. Also, we regard that different agents may have different reverberation kernels, thus reflecting their preference differences.

A reverberation transform, denoted as  $\mathcal{R}_{(\mathbf{R},\mathbf{G})}[\cdot]$ , transforms similarity  $\mathbf{F}$  from the *observation* domain (corresponding to  $T_h$  past steps) into the *rehearsal* domain (plan-previews for future  $T_f$  steps). For the dth feature dimension, the transformed slice  $\mathbf{F}_{::d} \in \mathbb{R}^{K_g \times T_f}$  is computed as the linear combination

$$\overline{\mathbf{F}}_{::d} = \mathcal{R}_{(\mathbf{R},\mathbf{G})} \left[ \mathbf{F}_{::d} \right] := \mathbf{G}^{\top} \mathbf{F}_{::d} \mathbf{R}. \tag{2}$$

For clarity, the tensor slicing operator ::d will be omitted hereafter, while the matrix multiplications for all feature dimensions will default to being broadcasted.

- 3) Interpretations of Reverberation Kernels: Reverberation transform can be interpreted as constructing a new set of adaptive kernels for trajectory prediction, where the reverberation kernel **R** characterizes event-level latencies, while the generating kernel **G** models global latency preferences and their stochastic variations. Together, these two kernels could span a representation space for trajectory-changing events, enabling an approximate completeness¹ for simulating latencies when planning trajectories. The reverberation transform can be separated as two sequential steps:
- (a) The reverberation kernel  $\mathbf{R}$  first linearly combines columns in each slice  $\mathbf{F}_{::d}$  to directly establish connections from every observation step  $t_{\mathrm{obs}} \in \{1,...,t_h\}$  to every future step  $t_{\mathrm{fut}} \in \{t_h+1,...,t_h+t_f\}$ . Each element  $\mathbf{R}_{uv}$  represents how an observed step  $t_{\mathrm{obs}} = u$  affects or contributes to the

TABLE I Symbols and network structures of the Rev model.

Sym.	Descriptions	Shapes
$egin{array}{c} \Delta t \\ \mathbf{p}_t^i \\ \mathbf{X}^i \\ \mathbf{Y}^i \end{array}$	Temporal interval to sample trajectories Agent-i's 2D position at time step $t$ i's observed trajectory ( $t_h$ past steps) i's groundtruth trajectory ( $t_f$ future steps)	$(m := 2)$ $(t_h, m)$ $(t_f, m)$
$d \\ N_{ heta} \\ K_{g} \\ \hat{\mathbf{Y}}_{R}^{i}$	Feature dimensions in most networks The number of social partitions The number of columns in generating kernels $Rev$ predictions ( $K_g$ generations each)	$\begin{matrix} -\\ -\\ -\\ (K_g,t_f,m) \end{matrix}$

future step  $t_{\rm fut}=t_h+v$ , reflecting how the planned timesensitive events are sourced from their causes during observation and scheduled after specific latencies. This formally enforces causal consistency between observations and future trajectory changes, making sure that agents' future steps are all sourced from their former states. For each feature dimension, it outputs a slice  $\mathbf{F}_{::d}\mathbf{R} \in \mathbb{R}^{T_h \times T_f}$ , which shares the same temporal scales and sequential length as the final predicted trajectory, especially without further recurrent computations.

(b) The generating kernel G then re-weights each row in the slice  $(\mathbf{F}_{::d}\mathbf{R})$  in  $K_q$  manners, simulating  $K_q$  different ways to handle such latencies in the rehearsal domain. This is inspired by the previous work MSN [6] that employs multiple style channels when forecasting to forecast better stochastic trajectories. In contrast, the generating kernel provides more alternatives for combining all historical trajectory-changing events with different latency preferences. Unlike the stylechannel-based MSN, such re-weights through the explicit kernel decomposition may not significantly diversify trajectorylevel outputs, but more ways to take into account latencies of all steps or events simultaneously. Formally, each of the  $K_q$ rows in G corresponds to a distinct latency-handling mode, which can be treated as minor but characteristic modifications to the reverberation kernel R to alter latency preferences. For each feature dimension, it outputs the slice  $\overline{\mathbf{F}}_{::d} \in \mathbb{R}^{K_g \times T_f}$ .

Overall, the reverberation transform is a feature-level mapping  $\mathcal{R}_{(\mathbf{R},\mathbf{G})}: \mathbb{R}^{T_h \times T_h \times D} \to \mathbb{R}^{K_g \times T_f \times D}$ . It maps the observed sequential representation  $\mathbf{f}$  (or similarity  $\mathbf{F} = \sigma(\mathbf{f})$ ) into the rehearsal domain to simulate agents' instant preview of their scheduled plans in the following  $T_f$  steps by explicitly taking into account latencies of trajectories-changing events, also their  $K_g$  potential variations of combinations. This design enables explicit modeling of heterogeneous latency preferences, which distinguishes the reverberation transform from existing feature-aggregation or style-based methods.

#### B. The Reverberation (Rev) Trajectory Prediction Model

**Formulations.** Building upon the reverberation transform, we now formulate the complete *Reverberation* (short for *Rev*) trajectory prediction model. Our main focus is to learn and forecast agents' latencies to handle trajectory-changing events when forecasting their trajectories, whether non-interactive or social events. Denote the 2D position (we use m=2 to represent this dimension) of any ith  $(i \in \{1, 2, ..., N_a\})$  agent at a time step t as  $\mathbf{p}_t^i = (x_t^i, y_t^i)^{\top} \in \mathbb{R}^2$ , our focused trajectory

<sup>&</sup>lt;sup>1</sup>See discussions of their theoretical properties in Appendix A.

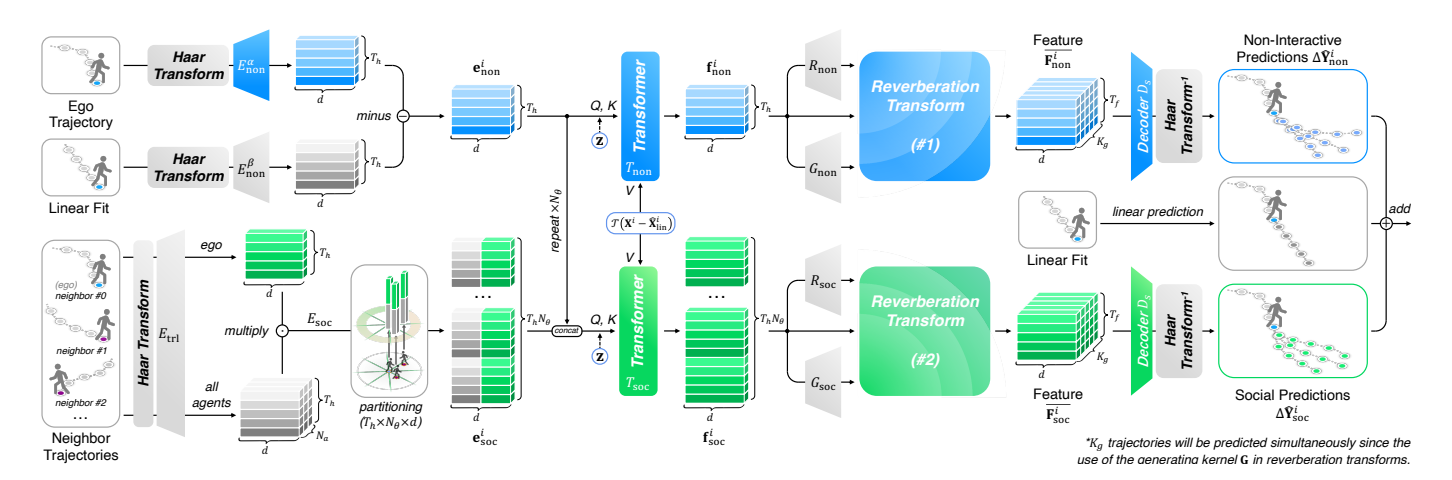


Fig. 3. Overview of the proposed *Reverberation* (short for *Rev*) trajectory prediction model. It predicts trajectories as two learnable parts for any ego i, the non-interactive  $\Delta \hat{\mathbf{Y}}_{\text{non}}^i$  and the social  $\Delta \hat{\mathbf{Y}}_{\text{soc}}^i$ , with specific non-interactive latencies and social latencies, added upon the linear prediction  $\hat{\mathbf{Y}}_{\text{lin}}^i$  as reference.

TABLE II NETWORK STRUCTURES AND COMPUTATIONS OF THE Rev MODEL.

Symbols	Descriptions
$\mathcal{T}(\cdot)$ $\mathcal{T}^{-1}(\cdot)$	Haar transform, $(t_h, m) \to (T_h, M)$ Inverse Haar transform, $(T_f, M) \to (t_f, m)$
$T_{\mathrm{non}}$	Transformer (4 encoder-decoder layers, 8 heads)
$T_{ m soc}$	Transformer (2 encoder-decoder layers, 8 heads)
$E_{ m non}^{lpha(eta)}$ / $E_{ m trl}$	$\rightarrow fc(d, ReLU) \rightarrow fc(d, tanh)$
$E_{ m soc}$	$\rightarrow \text{fc}(d, \text{ReLU}) \rightarrow \text{fc}(d, \text{ReLU}) \rightarrow \text{fc}(d/2, \text{ReLU})$
$R_{\rm non}$ or $R_{\rm soc}$	$\rightarrow \text{fc}(d, \text{ReLU}) \rightarrow \text{fc}(d, \text{ReLU}) \rightarrow \text{fc}(T_f, \text{tanh})$
$G_{\text{non}}$ or $G_{\text{soc}}$	$\rightarrow \text{fc}(d, \text{ReLU}) \rightarrow \text{fc}(d, \text{ReLU}) \rightarrow \text{fc}(K_g, \text{tanh})$
$D_{\text{non}}$ or $D_{\text{soc}}$	$\rightarrow fc(M, none)$

prediction aims at forecasting possible future trajectory(ies)  $\hat{\mathbf{Y}}^i = (\hat{\mathbf{p}}_{t_h+1}^i,...,\hat{\mathbf{p}}_{t_h+t_f}^i)^\top \in \mathbb{R}^{t_f \times 2} \text{ on } t_f \text{ discrete future steps, according to the observed trajectories of all these agents } \mathcal{X} = \{\mathbf{X}^i = (\mathbf{p}_1^i,...,\mathbf{p}_{t_h}^i)^\top \in \mathbb{R}^{t_h \times 2} | i=1,2,...,N_a\} \text{ on the currently observed } t_h \text{ steps (all temporal steps are sampled with the interval } \Delta t). Formally, it aims at constructing the network <math>N$ , such that  $\{\hat{\mathbf{Y}}^i\} = N(\mathcal{X})$ . Summaries of symbols and network structures are listed in Tabs. I and II.

**Method Details.** Inspired by the *Resonance* [21] model that divides trajectory prediction into the forecasting of decoupled vibration potions, we use a similar structure to organize our prediction pipeline. Like *Resonance*, *Rev* predicts trajectories as three decoupled portions: linear trajectory, non-interactive trajectory, and social trajectory, so that different kinds of latencies could be separately learned and decoupledly considered. As illustrated in Fig. 3, for any ego agent i, a batch of prediction  $\hat{\mathbf{Y}}_R^i$  is forecasted by

$$\hat{\mathbf{Y}}_{R}^{i} = \hat{\mathbf{Y}}_{\text{lin}}^{i} + \Delta \hat{\mathbf{Y}}_{\text{non}}^{i} + \Delta \hat{\mathbf{Y}}_{\text{soc}}^{i}.$$
 (3)

Here, each  $\hat{\mathbf{Y}}_R^i \in \mathbb{R}^{K_g \times t_f \times 2}$  contains a batch of stochastic predictions ( $K_g$  forecasted trajectories for each ego i, where we use the tensor slice  $\hat{\mathbf{Y}}_{k::}^i$  to denote each kth prediction).

1) Linear Predictions: Inspired by the Resonance model [21], the uniform (linear) movement of ego agents without external forces will be considered as a reference for considering and modeling both non-interactive or social latencies and

corresponding predictions. Such linear fit  $\hat{\mathbf{X}}_{\mathrm{lin}}^i \in \mathbb{R}^{t_h \times 2}$  and linear prediction  $\hat{\mathbf{Y}}_{\mathrm{lin}}^i \in \mathbb{R}^{t_f \times 2}$  are computed by

$$\hat{\mathbf{X}}_{\text{lin}}^{i} = \mathbf{A}_{h} \mathbf{w}_{\text{lin}}^{i} = \begin{pmatrix} 1 & 1 & \dots & 1 \\ 1 & 2 & \dots & t_{h} \end{pmatrix}^{\top} \mathbf{w}_{\text{lin}}^{i}, \tag{4}$$

$$\hat{\mathbf{Y}}_{\text{lin}}^i = \mathbf{A}_f \mathbf{w}_{\text{lin}}^i = \begin{pmatrix} 1 & \dots & 1 \\ t_h + 1 & \dots & t_h + t_f \end{pmatrix}^\top \mathbf{w}_{\text{lin}}^i.$$
 (5)

Here,  $\mathbf{w}_{\mathrm{lin}}^i \in \mathbb{R}^{2 \times 2}$  is the linear weights, solved by

$$\mathbf{w}_{\text{lin}}^{i} = \left(\mathbf{A}_{h}^{\top} \mathbf{A}_{h}\right)^{-1} \mathbf{A}_{h}^{\top} \mathbf{X}^{i}. \tag{6}$$

2) Non-interactive Latencies: We now focus on the latencies of (ego) agents themselves to handle their own trajectory-changing events, including the intention changes or random behaviors during the observation period. We first construct representations of such non-interactive part of any ego-i's observed trajectory  $\mathbf{X}^i$ . This residual term describes how agents' observed trajectories differ from their initial plans (linear movements) after self-sourced trajectory-changing events. Given two mirrored embedding MLPs  $E_{\mathrm{non}}^{\alpha}$  and  $E_{\mathrm{non}}^{\beta}$  (structures in Tab. II), we have

$$\mathbf{e}_{\text{non}}^{i} = \frac{1}{2} \left[ E_{\text{non}}^{\alpha} \left( \mathcal{T}[\mathbf{X}^{i}] \right) - E_{\text{non}}^{\beta} \left( \mathcal{T}[\hat{\mathbf{X}}_{\text{lin}}^{i}] \right) \right]. \tag{7}$$

Here,  $\mathcal{T}$  denotes the Haar transform that maps trajectories into the frequency domain, since previous work [21] has indicated its capability in characterizing sequences from the time-frequency joint distribution perspective, which may help us model latency preferences. Considering that this transform will change the shape of the sequences, we denote the size of Haar spectrums with capitalized symbols, like the mapping of shapes  $(t_h, m) \rightarrow (T_h := t_h/2, M := 2m)$ (m is the dimension of trajectories, which is constantly set to 2 in this manuscript for handling 2D trajectories). Denote the feature dimension as d, we have  $\mathbf{e}_{\text{non}}^i \in \mathbb{R}^{T_h \times d}$ . Therefore, the minimum unit for encoding and processing these self-sourced trajectory-changing events has become each observation step in the frequency domain (Haar), i.e., each temporal-spectral step, corresponding to adjacent 2 real-world observation frames.

A Transformer [60] backbone  $T_{\rm non}$  will be used to establish relations between different temporal (spectral) steps for the embedded  $\mathbf{e}_{\rm non}^i$ . Here,  $\mathbf{e}_{\rm non}^i$  itself acts as both keys and queries for computing attention in both Transform encoder and decoder, while the differential spectrum  $\mathcal{T}[\mathbf{X}^i - \hat{\mathbf{X}}_{\rm lin}^i]$  will play the target value of queries in the Transform decoder. A noise  $\mathbf{z}_{\rm non} \sim \mathbf{N}(\mathbf{0}, \mathbf{I})$  will be sampled at each run to simulate random choices. It finally encodes a feature  $\mathbf{f}_{\rm non}^i \in \mathbb{R}^{T_h \times d}$ :

$$\mathbf{f}_{\text{non}}^{i} = T_{\text{non}} \left( \text{Concat} \left( \mathbf{e}_{\text{non}}^{i}, \mathbf{z}_{\text{non}} \right), \mathcal{T} [\mathbf{X}^{i} - \hat{\mathbf{X}}_{\text{lin}}^{i}] \right).$$
 (8)

Then, the reverberation transform  $\mathcal{R}_{(\mathbf{R}_{\mathrm{non}}^i, \mathbf{G}_{\mathrm{non}}^i)}$  will be applied to transform feature  $\mathbf{f}_{\mathrm{non}}^i$  into the rehearsal domain, denoted as  $\overline{\mathbf{F}^i}_{\mathrm{non}}$ , with two trainable reverberation kernels  $\mathbf{R}_{\mathrm{non}}^i$  and  $\mathbf{G}_{\mathrm{non}}^i$  assigned for each agent. This reverberation transform is a feature-level map  $\mathbb{R}^{T_h \times T_h \times d} \to \mathbb{R}^{K_g \times T_f \times d}$ . Given two MLPs  $R_{\mathrm{non}}$  and  $G_{\mathrm{non}}$  (see Tab. II), we have

$$\mathbf{R}_{\text{non}}^{i} = R_{\text{non}} \left( \mathbf{f}_{\text{non}}^{i} \right), \quad \mathbf{G}_{\text{non}}^{i} = G_{\text{non}} \left( \mathbf{f}_{\text{non}}^{i} \right), \qquad (9)$$

$$\overline{\mathbf{F}_{\text{non}}^{i}} = \mathcal{R}_{\left( \mathbf{R}_{\text{non}}^{i}, \mathbf{G}_{\text{non}}^{i} \right)} \left[ \sigma \left( \mathbf{f}_{\text{non}}^{i} \right) \right] \in \mathbb{R}^{K_{g} \times T_{f} \times d}. \qquad (10)$$

The final **non-interactive prediction**  $\Delta \hat{\mathbf{Y}}_{\mathrm{non}}^{i}$  is inferred from such rehearsal representation  $\overline{\mathbf{F}_{\mathrm{non}}^{i}}$  via a simple decoder MLP  $D_{\mathrm{non}}$  (an FC layer without activations, see Tab. II). After applying the inverse trajectory transform  $\mathcal{T}^{-1}$ , we have

$$\Delta \hat{\mathbf{Y}}_{\text{non}}^{i} = \mathcal{T}^{-1} \left[ D_{\text{non}} \left( \overline{\mathbf{F}_{\text{non}}^{i}} \right) \right] \in \mathbb{R}^{K_g \times t_f \times 2}.$$
 (11)

This process could be treated as the learning of potential biases between the scheduled trajectories during rehearsal and the actual trajectories observed after the prediction period. They share the same temporal scale and no additional extrapolations are required during forecasting. It can also be seen that the Transformer backbone only computes temporal features on the observation period during forecasting, rather than the entire observation and prediction periods. Compared to former works that utilize recurrent neural networks or Transformers to directly compute features from the observation to the whole prediction periods, the reverberation transform not only straightforwardly provides a "buffer pool" (the rehearsal representations) that aligns the prediction period, but also keeps the continuity during training and testing while avoiding further recurrent computations. Most importantly, the latency when agents react to different trajectory determinants and its randomness could still be accurately learned and captured from two trainable reverberation kernels. This is why the rehearsal domain and the reverberation transform have been introduced.

3) Social Latencies: Our considered social latencies indicate how agents schedule their responses to social behaviors, like how long to start noticing, handling, or finally finishing them. The corresponding social prediction is forecasted with similar pipelines to the above non-interactive prediction. Its difference is that representations of social interactions will be considered before encoding and forecasting.

Different from non-interactive latencies, it is inline with our intuition that agents may present distinctive latency preferences for handling social events that happened from different angular orientations. Inspired by works [21], [41] that represent social interactions in an angle-based space, we use a

similar social-interaction-modeling approach like proposed in Resonance [21] to represent the context of social interactions when forecasting. It divides the whole  $2\pi$  angle into  $N_{\theta}$  anglebased social partitions, and computes the average dot product between the features of each neighbor and the ego within every partition to represent social interactions. For any agent u, its feature is first embedded into the  $\mathbf{e}_{\text{trl}}^u \in \mathbb{R}^{T_h \times d}$  through the translated trajectory  $\mathbf{X}^u - \mathbf{p}_{th}^u$ , via MLP  $E_{\text{trl}}$  in Tab. II:

$$\mathbf{e}_{\text{trl}}^{u} = E_{\text{trl}} \left( \mathcal{T} \left[ \mathbf{X}^{u} - \mathbf{p}_{t_{h}}^{u} \right] \right). \tag{12}$$

Then, for the ego i, considering a neighbor j, their interactions are encoded and represented as spectral similarity [21]

$$\mathbf{e}_{\text{soc}}^{i \leftarrow j} = E_{\text{soc}} \left( \mathbf{e}_{\text{trl}}^{i} \odot \mathbf{e}_{\text{trl}}^{j} \right), \tag{13}$$

where  $\odot$  denotes the element-wise multiply  $(\mathbf{e}_{\mathrm{soc}}^{i \leftarrow j} \in \mathbb{R}^{T_h \times d})$ .

After that, all ego-neighbor-pair's representations will be averaged within each social partition. The following computations are the same as those used in the *Resonance* model [21], by replacing their " $\mathbf{f}^{i\leftarrow j}$ " with the above " $\mathbf{e}^{i\leftarrow j}$ " in their original Eqs. (11) - (12). Similar to their resonance matrix, we have our social representation  $\mathbf{e}^i_{\text{soc}} \in \mathbb{R}^{T_h \times N_\theta \times d}$ .

Compared to the original computations [21], the main difference is that the  $\mathbf{e}_{\mathrm{soc}}^i$  maintains both temporal-spectral ( $T_h$  historical steps) and spatial ( $N_{\theta}$  angular positions) information of all social events during observation, which ensures the locating and modeling of latencies to handle social events from the partition-level dynamically. In other words, the **minimum unit** for handling social trajectory-changing events has become one partition at each temporal-spectral step. This ensures that the reverberation kernels could account for angle-specific social interactions and their latencies, like different delays induced by neighbors in front versus behind the ego agent.

Then, social representation  $\mathbf{e}_{\mathrm{soc}}^i$  and the former embedded  $\mathbf{e}_{\mathrm{non}}^i$  will be further encoded together using another Transformer backbone  $T_{\mathrm{soc}}$ . To make such two representations compatible, the non-interactive  $\mathbf{e}_{\mathrm{non}}^i$   $(T_h \times d)$  will be repeated for  $N_{\theta}$  times and then concatenated into its first dimension, turning it into the new representation  $\tilde{\mathbf{e}}_{\mathrm{non}}^i \in \mathbb{R}^{T_h N_{\theta} \times d}$ . Meanwhile, the first two dimensions of the social  $\mathbf{e}_{\mathrm{soc}}^i$   $(T_h \times N_{\theta} \times d)$  will be flattened, turning into the compatible  $\tilde{\mathbf{e}}_{\mathrm{soc}}^i \in \mathbb{R}^{T_h N_{\theta} \times d}$ . Then, like Eq. (8), sample noise  $\mathbf{z}_{\mathrm{soc}} \sim \mathbf{N}(\mathbf{0}, \mathbf{I})$ , we have

$$\mathbf{f}_{\text{soc}}^{i} = T_{\text{soc}} \left( \text{Concat} \left( \tilde{\mathbf{e}}_{\text{non}}^{i}, \tilde{\mathbf{e}}_{\text{soc}}^{i}, \mathbf{z}_{\text{soc}} \right), \mathcal{T} [\mathbf{X}^{i} - \hat{\mathbf{X}}_{\text{lin}}^{i}] \right).$$
(14)

Similar to Eq. (10), reverberation transform  $\mathcal{R}_{(\mathbf{R}_{\mathrm{soc}}^i, \mathbf{G}_{\mathrm{soc}}^i)}$  is then applied on feature  $\mathbf{f}_{\mathrm{soc}}^i$  along with its two trainable reverberation kernels  $\mathbf{R}_{\mathrm{soc}}^i$  and  $\mathbf{G}_{\mathrm{soc}}^i$ . Differently, this reverberation transform is a map:  $\mathbb{R}^{T_hN_\theta\times T_hN_\theta\times d}\to\mathbb{R}^{K_g\times T_f\times d}$ , aiming at locating social events both temporally and spatially. These kernels are inferred from MLPs  $R_{\mathrm{soc}}$  and  $G_{\mathrm{soc}}$  (Tab. II):

$$\mathbf{R}_{\mathrm{soc}}^{i} = R_{\mathrm{soc}}\left(\mathbf{f}_{\mathrm{soc}}^{i}\right), \quad \mathbf{G}_{\mathrm{soc}}^{i} = G_{\mathrm{soc}}\left(\mathbf{f}_{\mathrm{soc}}^{i}\right), \quad (15)$$

$$\overline{\mathbf{F}_{\text{soc}}^{i}} = \mathcal{R}_{(\mathbf{R}_{\text{soc}}^{i}, \mathbf{G}_{\text{soc}}^{i})} \left[ \sigma(\mathbf{f}_{\text{soc}}^{i}) \right] \in \mathbb{R}^{K_{g} \times T_{f} \times d}.$$
 (16)

Given the decoder  $D_{\text{soc}}$  (same structured as  $D_{\text{non}}$ ), social **prediction**  $\Delta \hat{\mathbf{Y}}_{\text{soc}}^i$  is forecasted by

$$\Delta \hat{\mathbf{Y}}_{\text{soc}}^{i} = \mathcal{T}^{-1} \left[ D_{\text{soc}} \left( \overline{\mathbf{F}_{\text{soc}}^{i}} \right) \right] \in \mathbb{R}^{K_g \times t_f \times 2}.$$
 (17)

4) Loss Function: Similar to previous works [6], to fore-cast better trajectories while maintaining its generalizability, Rev model is trained end-to-end with the best-of- $K_g$   $\ell_2$  loss. For the ego agent i, considering the batch of predictions ( $\hat{\mathbf{Y}}^i$  outputted during once forwarding and noise-sampling, containing  $K_g$  stochastic trajectories in total) and the ground truth trajectory  $\mathbf{Y}^i$ , this loss function L is computed as

$$L\left(\hat{\mathbf{Y}}^{i}, \mathbf{Y}^{i}\right) = \min_{1 \le k \le K_g} \frac{1}{t_f} \left\| \hat{\mathbf{Y}}_{k::}^{i} - \mathbf{Y}^{i} \right\|_{2}. \tag{18}$$

# IV. EXPERIMENTS

#### A. Experimental Settings

- 1) Datasets: We use three public trajectory datasets<sup>2</sup> to evaluate the proposed Rev model, including two pedestrian sets (ETH-UCY and SDD) and one vehicle dataset (nuScenes):
- (a) **ETH** [61]-UCY [62] contains several pedestrian walking scenes, including five main test scenes: eth, hotel, univ, zara1, zara2. Models are validated with *leave-one-out* [1], [14] strategy, under the common  $\{t_h, t_f, \Delta t\} = \{8, 12, 0.4\}$  settings.
- (b) **Stanford Drone Dataset** (**SDD**) [63] contains 60 drone videos captured in the Stanford campus. Multiple kinds of agents, like pedestrians, bikers, and carts, have been labeled, presenting more complex interactions. We randomly select 36 videos to train, 12 to validate, and the left 12 to test [64] [65], also using the common  $\{t_h, t_f, \Delta t\} = \{8, 12, 0.4\}$  settings.
- (c) **nuScenes** [66] is a large-scale dataset collected from urban driving scenes, including multiple kinds of vehicles and pedestrians. We use 550 scenes to train, 150 to validate, and 150 to test [67]. Only vehicles' trajectories are used [34], with the  $\{t_h, t_f, \Delta t\} = \{4, 12, 0.5\}$  settings [68].
- 2) Metrics: We use the best Average/Final Displacement Error over K generated trajectories [1], [14], [61] to evaluate models' performance, known as "minADE $_K$ /minFDE $_K$ ", where K is usually set to 20 when evaluating. For agent i, using subscript  $_k$  to denote kth prediction, we have

$$\min \text{ADE}_{20}(i) = \min_{k \in \{1, 2, \dots, K\}} \frac{1}{t_f} \sum_{t=t_h+1}^{t_h+t_f} \left\| \hat{\mathbf{p}}_{t_k}^i - \mathbf{p}_t^i \right\|_2, \quad (19)$$

$$\min \text{FDE}_{20}(i) = \min_{k \in \{1, 2, \dots, K\}} \left\| \hat{\mathbf{p}}_{t_h + t_f}^i - \mathbf{p}_{t_h + t_f}^i \right\|_2. \quad (20)$$

The final metrics are averaged over every agent in each set, and we will refer to them as "ADE/FDE" for clarity.

In addition, we have proposed a qualitative metric, named *reverberation strength*, to characterize agents' latencies for handling trajectory-changing events. This metric helps us locate and evaluate the latency of each event when forecasting. See detailed formulations and discussions in Sec. IV-D.

3) Baselines: We choose several recent state-of-the-art methods as our baselines, including SHENet [69], MID [17], RAN [70], MS-TIP [71], SMEMO [72], LG-Traj [73], MSRL [74], PPT [75], E-V<sup>2</sup>-Net [76], AngetFormer [34], SocialCircle [40], SocialCircle+ [41], Y-net [77], UPDD [78], Resonance [21], FlowChain [79], IMP [80], SpecTGNN [81], UEN

 $^2$ We also use a motion (human skeleton) prediction dataset to verify the generalizability of Rev beyond trajectory prediction. See Appendix C.

- [82], MUSE-VAE [68], Trajectron++ [83], SoperModel [84], Dice [55], and AgentFormer-FLN [85].
- 4) Implementation Details: The proposed Rev model is trained on one NVIDIA RTX 3090, using an Adam optimizer with a learning rate of 3e-4 and a batch size of 1000 for up to 200 epochs. When generating 20 trajectories, the number of columns of generating kernels G is set to  $K_g = 20$ . Feature dimension of most subnetworks is set to d = 128. According to conclusions of previous research [21], [40], [41], the number of social partitions is set to  $N_\theta = 8$ . Trajectories of ego agents have been translated to the origin as a preprocess [76] before the network implementation. All reported ADE/FDE results are averaged across five runs. Model weights of Rev models and ablation variations, training code and detailed training settings have been provided in our code repo.

# B. Comparisons to State-of-the-Arts

This section quantitatively compares the *Rev* model with several recent published state-of-the-art methods on multiple datasets. Results (ADE/FDE<sup>3</sup>) are reported in Tabs. III and IV.

**Pedestrian Datasets:** It should be noted that the prediction improvements on these two pedestrian datasets have become increasingly marginal in recent years, approaching a potential bottleneck. Under such conditions, the proposed Rev model still demonstrates competitive performance. In Tab. III, it can be seen that Rev could obtain top-3 prediction performance on all five ETH-UCY sets, presenting its adaptivity across different scenes. Interestingly, its results on the univ or zara2 outperform most methods, which performs the level as recent baselines like SocialCircle+ and PPT on univ while outperforms the UPDD for about 29% FDE on zara2, highlighting its strengths on dense scenes. Also, its performance gains are more balanced for both ADE and FDE, indicating that either global trends or trajectory destinations could be taken into account simultaneously. Notably, Rev outperforms the state-of-the-art Resonance for about 2.1% lower ADE and 1.5% lower FDE, and about 3.5% lower ADE against the other MUSE-VAE, where such improvements are rarely seen even on SDD. This demonstrates its adaptability to diverse pedestrian scenarios, whether on streets or campuses.

**Vehicle Dataset:** Tab. **IV** shows that *Rev* also presents noticeable performance gains on the vehicle dataset. When generating K=10 trajectories, it outperforms *Resonance* for about 4.2% FDE. Our above observations also apply to this vehicle dataset that both global trends (ADE) and destinations (FDE) considerations could be balanced for the proposed *Rev*. For example, comparing *Resonance* and MUSE-VAE, the former one presents lower ADE while the other has lower FDE. Meanwhile, *Rev* has 2.9% lower ADE and 3.3% FDE than both of them. Note that *Rev* performs slightly worse than *Resonance* (0.8%/0.4% worse ADE/FDE) when only generating K=5 trajectories, revealing potential shortcomings when generating a limited number of trajectories. Nevertheless, it still outperforms MUSE-VAE for about 9.4%/9.3% of ADE/FDE under this situation, presenting its competitiveness.

<sup>&</sup>lt;sup>3</sup>See statistical verifications of metrics in Appendix D.

TABLE III

COMPARISONS WITH OTHER STATE-OF-THE-ARTS ON ETH-UCY (LEFT) AND SDD (RIGHT). METRICS ARE REPORTED IN THE FORM OF "ADE/FDE" (best-of-20). LOWER METRICS INDICATE BETTER PREDICTION PERFORMANCE. BLUE MARKERS DENOTE THE BEST 3 RESULTS ON EACH SET.

Method (ETH-UCY)	eth ↓	hotel ↓	univ ↓	zara1 ↓	zara2 ↓	Average ↓	Method (SDD)	ADE/FDE ↓
SHENet [69] (2022)	0.41/0.61	0.13/0.20	0.25/0.43	0.21/0.32	0.15/0.26	0.23/0.36	RAN [70] (2024)	10.97/19.95
MID [17] (2022)	0.39/0.66	0.13/0.22	0.22/0.45	0.17/0.30	0.13/0.27	0.21/0.38	FlowChain [79] (2023)	9.93/17.17
RAN [70] (2024)	0.41/0.69	0.13/0.21	0.25/0.46	0.22/0.41	0.16/0.31	0.23/0.42	IMP [80] (2023)	8.98/15.54
MS-TIP [71] (2024)	0.39/0.57	0.13/0.22	0.24/0.40	0.20/0.34	0.17/0.29	0.22/0.36	SpecTGNN [81] (2021)	8.21/12.41
SMEMO [72] (2024)	0.39/0.59	0.14/0.20	0.23/0.41	0.19/0.32	0.15/0.26	0.22/0.35	SMEMO [72] (2024)	8.11/13.06
LG-Traj [73] (2024)	0.38/0.56	0.11/0.17	0.23/0.42	0.18/0.33	0.14/0.25	0.20/0.34	LG-Traj [73] (2024)	7.80/12.79
MSRL [74] (2023)	0.28/0.47	0.14/0.22	0.24/0.43	0.17/0.30	0.14/0.23	0.19/0.33	Y-net [77] (2021)	7.85/11.85
PPT [75] (2024)	0.36/0.51	0.11/0.15	0.22/0.40	0.17/0.30	0.12/0.21	0.20/0.31	UEN [82] (2024)	7.30/10.40
E-V <sup>2</sup> -Net [76] (2025)	0.25/0.38	0.11/0.16	0.23/0.42	0.19/0.30	0.13/0.24	0.18/0.30	PPT [75] (2024)	7.03/10.65
AngetFormer [34] (2021)	0.26/0.39	0.11/0.14	0.26/0.46	0.15/0.23	0.14/0.23	0.18/0.29	UPDD [78] (2024)	6.59/13.90
SocialCircle [40] (2024)	0.25/0.38	0.12/0.14	0.23/0.42	0.18/0.29	0.13/0.22	0.18/0.29	E-V <sup>2</sup> -Net [76] (2025)	6.57/10.49
SocialCircle+ [41] (2024)	0.25/0.39	0.10/0.15	0.24/0.42	0.18/0.28	0.13/0.22	0.18/0.29	SocialCircle [40] (2024)	6.54/10.36
Y-net [77] (2021)	0.28/0.33	0.10/0.14	0.24/0.41	0.17/0.27	0.13/0.22	0.18/0.27	SocialCircle+ [41] (2024)	6.44/10.22
UPDD [78] (2024)	0.22/0.42	0.17/0.30	0.14/0.28	0.16/0.30	0.14/0.31	0.17/0.32	MUSE-VAE [68] (2022)	6.36/11.10
Resonance [21] (2025)	0.23/0.35	0.10/0.15	0.24/0.41	0.17/0.29	0.13/0.22	0.17/0.28	Resonance [21] (2025)	6.27/10.02
Rev (Ours)	0.23/0.34	0.10/0.15	0.23/0.40	0.17/0.28	0.13/0.22	0.17/0.28	Rev (Ours)	6.14/9.87

TABLE IV

COMPARISONS TO OTHER STATE-OF-THE-ARTS ON NUSCENES. METRICS REPORTED ARE "ADE/FDE" IN METERS UNDER best-of-5 AND best-of-10.

BLUE MARKERS DENOTE THE BEST 3 RESULTS UNDER EACH SETTING.

Method (nuScenes)	best-of-5 $\downarrow$	best-of-10 $\downarrow$
Trajectron++ [83] (2020)	3.14/7.45	2.46/5.65
Y-net [77] (2020)	2.46/5.15	1.88/3.47
SoperModel [84] (2025)	2.21/4.58	1.79/3.40
AngetFormer [34] (2021)	1.86/3.89	1.45/2.86
Dice [55] (2024)	1.76/3.70	1.44/2.67
AgentFormer-FLN [85] (2024)	1.83/3.78	1.32/2.73
E-V <sup>2</sup> -Net [76] (2025)	1.46/3.18	1.15/2.37
SocialCircle [40] (2024)	1.44/3.10	1.13/2.30
MUSE-VAE [68] (2022)	1.38/2.90	1.09/2.10
Resonance [21] (2025)	1.26/2.72	1.03/2.12
Rev (Ours)	1.25/2.73	1.00/2.03

#### C. Ablation Studies

This section conducts ablation studies to verify how each proposed component works in the *Rev* model. Detailed ablation settings and results are reported in Tabs. V and VI. (Reported results are averaged over 5 runs to reduce randomness.)

1) Overall Verifications of Reverberation Transform: We use a series of minimal variations {a1, a2, a3, a4} to verify how the reverberation transform helps to achieve better performance. These variations only include a single Transformer backbone to make predictions. They do not include any further operations like decoupling prediction into non-interactive or social portions, with only social-interaction-modeling components reserved. We observe from Tabs. V and VI that the use of reverberation transform could directly lead to better quantitative performance, especially by using its two kernels R and G simultaneously. Especially, it can be seen that this transform may bring lower FDEs. For example, variation a4 outperforms a1 for up to 5.7% FDE on eth and 12.7% FDE on univ. Variation a4 also brings noticeable ADE enhancements, including about 3.3% on the average of ETH-UCY, 1.4% on SDD, and 19.6% on nuScenes (best-of-10), although such enhancements are not that strong as those in FDE (7.8%,

- 4.2%, and 26.3%, respectively). These results could verify the usefulness of the reverberation transform, especially in forecasting trajectories in the further future, where all latencies have been posted intuitively for better FDE gains than ADE.
- 2) Verifications of Reverberation Kernel R: This kernel serves as the main role to map features from the observation domain into the rehearsal domain, learning initial causalities and latencies for handling trajectory-changing events. Comparing variation-pairs {a3, a4} or {a10, full} in Tabs. V and VI, similar to our above conclusions, it can be seen that FDEs have been far improved than ADEs, like 8.6%/12.0% gains on ETH-UCY (a3 and a4), indicating the potential relationship between this reverberation kernel and latencies in the further future. Variations {a10, full} show similar trends, including 4.4%/7.8% gains on ETH-UCY and 2.9%/4.9% on SDD. These results could prove that the reverberation kernel R plays the core role to consider how trajectories could grow in the further future, also prove the usefulness of directly modeling latencies of trajectory-changing events when forecasting.
- 3) Verifications of Generating Kernel G: This kernel provides randomness and alternatives to kernel R, simulating agents' unique stochastic properties of latencies. In variations a2 and a9, we use the MSN-like [6] strategy as comparisons when this kernel is disabled. Comparing variations {a9, full} in Tabs. V and VI, we see that kernel G achieves larger ADE improvements than kernel R, gaining for 3.9%/4.7% on ETH-UCY and even 1.0%/-1.8% on nuScenes (10). These comparisons indicate that the kernel G is better at improving the predicted trajectories globally (since its ADE gains), presenting a totally different role compared to the reverberation kernel R. Especially, we see that the use of kernel G even leads to a little worse FDE on nuScenes, which could be a compromise of prediction accuracy and diversity<sup>4</sup>.
- 4) Verifications of Non-interactive and Social Latencies: We use two paralleled networks to learn latencies of agents for handling non-interactive and social trajectory-changing

<sup>&</sup>lt;sup>4</sup>See further discussions in Sec. IV-E2 and Appendix A.

TABLE V

Ablation Studies on ETH-UCY and SDD. " $\mathcal{R}$ " denotes whether the reverberation transform is applied when forecasting, with whether or how kernels  $\mathbf{G}$  and  $\mathbf{R}$  are included. "lin", "non", and "soc" denotes whether linear predictions, non-interactive predictions, and social predictions are considered when training. Metrics reported are "ADE/FDE" using best-of-20. Blue numbers mark the top-3 results on each set, and underline numbers denote the best metrics.

ID	$\mathcal{R}$	G	R	lin non soc	eth	hotel	univ	zara1	zara2	ETH-UCY	SDD
a1	×	_	_	Forecast together	0.265/0.424	0.109/0.167	0.344/0.620	0.194/0.336	0.138/0.240	0.210/0.357	6.477/10.460
a2	$\checkmark$	×	$\checkmark$	Forecast together	0.269/0.395	0.114/0.171	0.387/0.692	0.196/0.315	0.142/0.238	0.222/0.362	6.381/10.095
a3	$\checkmark$	$\checkmark$	×	Forecast together	0.243/0.373	0.117/0.164	0.415/0.779	0.194/0.316	0.140/0.240	0.222/0.374	6.337/10.176
a4	$\checkmark$	$\checkmark$	$\checkmark$	Forecast together	0.265/0.401	0.110/0.161	0.310/0.541	0.191/0.314	0.141/0.231	0.203/0.329	6.386/10.022
a5	$\checkmark$	$\checkmark$	$\checkmark$	× ✓ ✓	0.273/0.380	0.108/0.160	0.337/0.593	0.190/0.299	0.138/0.227	0.209/0.332	6.296/10.064
a6	$\checkmark$	$\checkmark$	$\checkmark$	✓ × ✓	0.238/0.377	0.110/0.164	0.249/0.440	0.174/0.294	0.136/0.236	0.181/0.302	6.286/10.247
a7	$\checkmark$	$\checkmark$	$\checkmark$	✓ ✓ ×	0.228/0.363	0.109/0.176	0.241/0.426	0.176/0.297	0.134/0.224	0.178/0.297	6.227/10.046
a8	×	_	_	$\checkmark$ $\checkmark$	0.255/0.400	0.107/0.160	0.280/0.521	0.178/0.305	0.133/0.230	0.191/0.323	6.446/10.672
a9	$\checkmark$	×	$\checkmark$	$\checkmark$ $\checkmark$	0.235/0.360	0.112/0.158	0.250/0.439	0.175/0.296	0.132/0.227	0.181/0.296	6.176/9.896
a10	$\checkmark$	$\checkmark$	×	$\checkmark$ $\checkmark$ $\checkmark$	0.238/0.366	0.107/0.155	0.260/0.473	0.176/0.301	0.133/0.238	0.182/0.306	6.326/10.388
full	✓	✓	✓	<b>√ √ √</b>	0.229/ <u>0.347</u>	0.105/0.154	0.237/0.409	0.172/0.283	0.131/0.220	0.174/0.282	6.144/9.874

TABLE VI Ablation Studies on NuScenes (only vehicles, 4  $\to$  12 frames). Metrics are reported in the form of "ADE/FDE" in Meters.

ID	$\mathcal{R}$	G	R	lin non soc	best-of-5	best-of-10
a1	×	_	_	Forecast together	1.571/3.354	1.342/2.930
a2	$\checkmark$	X	$\checkmark$	Forecast together	1.339/2.897	1.107/2.236
a3	$\checkmark$	$\checkmark$	×	Forecast together	1.455/3.054	1.087/2.312
a4	$\checkmark$	$\checkmark$	$\checkmark$	Forecast together	1.320/2.836	1.078/2.160
a5	$\checkmark$	$\checkmark$	$\checkmark$	× √ √	1.257/2.734	1.002/2.025
a6	$\checkmark$	$\checkmark$	$\checkmark$	✓ × ✓	1.315/2.928	1.061/2.218
a7	✓	$\checkmark$	$\checkmark$	✓ ✓ ×	1.307/2.889	1.065/2.219
a8	×	_	_	× ✓ ✓	1.344/2.893	1.111/2.281
a9	✓	×	$\checkmark$	× ✓ ✓	1.308/2.897	1.050/2.170
a10	$\checkmark$	$\checkmark$	×	× ✓ ✓	1.309/2.861	1.054/2.188
full	✓	✓	✓	<b>√ √ √</b>	1.306/2.901	1.040/2.173

events and making the corresponding predictions. Comparing variations {a6, a7, full} in Tabs. V and VI, it can be seen that the use of both branches mostly leads to the best prediction performance. Specifically, removing the non-interactive branch from the full variation may lead to more performance drops than removing the social branch, like -4.0%/-7.0% versus -2.3%/-5.3% on ETH-UCY. Such a difference is consistent with our intuition that social behaviors may not significantly modify our scheduled trajectory, as discussed from the energy perspective from Resonance [21]. Nevertheless, both such branches could have still provided comparable performance gains compared to the "forecast-together" variation a4, with up to 14.3% gains on ETH-UCY. Similar trends could also be observed for the nuScenes results in Tab. VI, which also presents an interesting phenomenon that the linear part could make the prediction performance slightly worse in this vehicle dataset, verifying the adaptability of these two branches in adjusting their roles in different datasets dynamically.

# D. Discussions of Reverberations and Latencies

Latencies within trajectories, *i.e.*, how long will each agent take to notice, to start handling, or finally to mark as completed a trajectory-changing event when planning trajectories, are the main focus of this manuscript. We now try to provide intuitive descriptions and interpretations of how the proposed

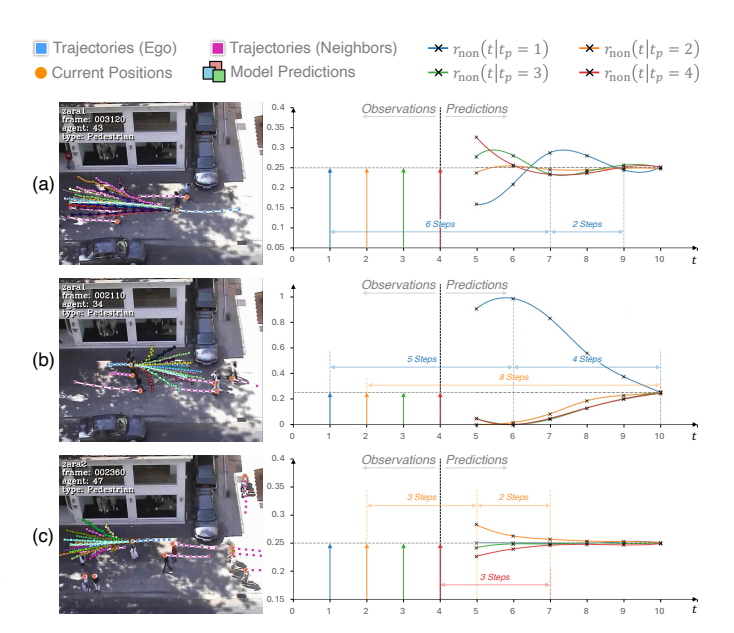


Fig. 4. Examples of non-interactive reverberation strength  $r_{\rm non}(t|t_p)$   $(t_p \in \{1,2,3,4\})$  of kernel  $\mathbf{R}_{\rm non}$  in the proposed *Rev* model.  $(\{T_h,T_f\}=\{4,6\})$ 

reverberation transform as well as the *Rev* model handle and forecast such focused latencies when forecasting trajectories.

As defined in Eq. (2), a reverberation transform  $\mathcal{R}_{(\mathbf{R},\mathbf{G})}$  is determined by one reverberation kernel  $\mathbf{R}$  and its corresponding generating kernel  $\mathbf{G}$ . In the proposed *Rev* model, we use two sets of such kernels,  $\{\mathbf{R}_{non}, \mathbf{G}_{non}\}$  and  $\{\mathbf{R}_{soc}, \mathbf{G}_{soc}\}^5$ , to learn and to forecast latencies of non-interactive and social trajectory-changing events correspondingly. We will first discuss non-interactive kernels, then social kernels.

According to the structure of *Rev*, for non-interactive latencies and predictions, the minimum unit for considering trajectory-changing events is an observation step, while a social partition at any observation step for social predictions. For clarity, we refer to "the feature of a minimum unit of trajectory-changing events" as "a trajectory-changing event".

<sup>&</sup>lt;sup>5</sup>Superscript <sup>i</sup> will be omitted for clarity when indicating agents' indices.

1) Non-Interactive Reverberation  $r_{\rm non}$ : Inspired by the reverberation curve in acoustics, we now define how latencies are represented from the reverberation kernels  ${\bf R}$ . Note that due to the use of Haar transform on trajectories [76] in Rev models, in the following discussions, our mentioned "one step" actually refers to 2 adjustment observation/prediction frames, i.e., 0.8 seconds on ETH-UCY or SDD. Therefore, the following discussions are conducted under  $\{T_h, T_f\} = \{4, 6\}$ , corresponding to the common  $\{t_h, t_f\} = \{8, 12\}$  setting.

The non-interactive reverberation curves aim at describing how a non-interactive, *i.e.*, self-sourced [21], trajectory-changing event, which happens at any past (observed) step  $t_p \in \{1,2,...,T_h\}$ , produces influences or contributes to the future trajectory at any future (prediction) step  $t_q \in \{T_h+1,T_h+2,...,T_h+T_f\}$ . The non-interactive reverberation kernel  $\mathbf{R}_{\mathrm{non}}$  is a 2D matrix with  $T_h$  rows and  $T_f$  columns, corresponding to  $T_h/T_f$  historical/future steps. For the ease of presentation, we denote the element (a real number) at  $t_p$ th row and  $(t_q-T_h)$ th column of matrix  $\mathbf{R}_{\mathrm{non}}$  as  $\mathbf{R}_{\mathrm{non}}[t_p,t_q]$ . Then, for an observed step  $t_p$ , given variable  $t \in \{T_h+1,...,T_h+T_f\}$ , we define the relative non-interactive reverberation strength  $r_{\mathrm{non}}(t|t_p)$  (we also call the non-interactive  $Reverberation\ Curve$  in our discussions) as

$$r_{\text{non}}(t|t_p) = \frac{(\mathbf{R}_{\text{non}}[t_p, t])^2}{\sum_{t_x=1}^{T_h} (\mathbf{R}_{\text{non}}[t_x, t])^2}.$$
 (21)

Fig. 4 visualizes several  $r_{\rm non}$  curves. It shows that Rev predicts far different latency-preferences for the ego agent to handle "self-sourced" trajectory-changing events on all historical steps. For example, in Fig. 4 (a), it considers that events occurring on the historical step 1 will be postponed<sup>6</sup> for about 6 steps (4.8s) to allow the ego agent to handle them. After that, such events will be paid the most concentration for about 2 steps (1.6s) to decide future trajectories, while other historical steps will be less concerned as a compromise. We can see from the left figure that the ego agent starts turning at step 1 (the first two observation frames). Such forecasted latencies could be explained as the prediction model regards that the agent may pay more attention to finish such turning before the step 7, and then reconsiders its future movements by taking into account where the turn is started and located. Differently, in Fig. 4 (b), it predicts events on step 1 will only take about 5 steps (4.0s) to nearly get that ego's *FULL* attention  $(r_{\text{non}}(6|1) \approx 1)$ for planning future trajectories, especially it has already been assigned a quite higher value at the first prediction step (step 5). The left figure shows that this ego agent starts moving from standing-still during the first four observation frames (2) steps, 1.6s). We can infer that Rev first predicts the ego to restore its walking status, then planning its further movements by simultaneously considering all past steps.

It also shows an interesting phenomenon that almost all historical steps will be considered to be paid the same attention in the further future, like after 5 prediction steps (4.0s) in Fig. 4 (a) and after 6 prediction steps (4.8s) in Fig. 4 (b). This

is inline with our intuition that all trajectory-changing events may only take effect within limited periods, especially when we are walking or behaving as pedestrians, though such effect may dramatically change the future path we selected. Also, such a conclusion also applies to Fig. 4 (c). It can be seen that every historical step contributes almost the same to all future steps when the ego pedestrian keeps moving at a static speed, where we can regard that no noteworthy trajectory-changing events have been captured during observation. We can verify from such non-interactive latency curves that the proposed reverberation transform has the ability to learn and to judge different latency preferences for different agents in handling those non-interactive trajectory-changing events.

2) Altered Non-Interactive Reverberation  $\tilde{r}_{non}$ : Generating kernel  $\mathbf{G}_{non}$  alters the original reverberation kernel  $\mathbf{R}_{non}$  in  $K_g$  ways to simulate randomness or variations of latencies for handling trajectory-changing events when forecasting. To better visualize such modifications, we define the non-interactive reverberation curves that are obtained after applying a generating kernel  $\mathbf{G}$  upon the corresponding reverberation kernel  $\mathbf{R}$  as the set of Altered Reverberation Curves to the original ones. Each set contains  $K_g$  altered but separated reverberation curves, symbolized with  $\tilde{r}_{non} = \{\tilde{r}_{non}^k\}_{k=1}^{K_g}$ , corresponding to  $K_g$  columns of the 2D matrix  $\mathbf{G}_{non}$ . Like above discussions, we use the symbol  $\mathbf{G}_{non}[t_p,k]$  to index matrix elements. Then, the kth ( $k \in \{1,2,...,K_g\}$ ) altered non-interactive reverberation strength (curve) is defined as

$$\tilde{r}_{\text{non}}^{k}(t|t_{p}) = \frac{\left(\mathbf{R}_{\text{non}}[t_{p}, t] \ \mathbf{G}_{\text{non}}[t_{p}, k]\right)^{2}}{\sum_{t_{x}=1}^{T_{h}} \left(\mathbf{R}_{\text{non}}[t_{x}, t] \ \mathbf{G}_{\text{non}}[t_{p}, k]\right)^{2}}.$$
 (22)

Fig. 5 visualizes several altered reverberation curves along with their original ones, corresponding to three prediction scenes in Fig. 4 (a), (b), and (c). Here, we observe that generating kernels may not significantly alter the trend of how a single historical event (step) is delayed or begins contributing to future trajectories, but provide alternative combinations that reflect how ego agents collectively consider latencies of all historical steps. In Fig. 5 (a0), it can be seen that step 1 is delayed to take effect until steps 7 and 8 (about 6 steps (4.8s) since step 1). Interestingly, such an increasing or decreasing trend of the reverberation strength  $r_{\rm non}(t|t_p=1)$  has been maintained in most of its altered ones (any  $\tilde{r}_{\rm non}^k(t|t_p=1)$ ), like generations (a2) (a3) (a5) and (a11) that all assign the most concentration for the historical step 1 at the future step 7. Compared to the original curves, the main difference is that latencies of different historical steps are balanced in obviously different ways after applying this generating kernel  $G_{non}$ . For example, considering all historical steps, the step 1 has been paid the most attention in generation (a2), while the minimum in generation (a12). Such results could verify the effectiveness of generating kernels on providing multiple latency preferences in the reverberation transform.

We can conclude that the role of a reverberation kernel  $\mathbf{R}_{\mathrm{non}}$  is to learn latencies for different ego agents to handle trajectory-changing events on each single historical step finely, while a generating kernel  $\mathbf{G}_{\mathrm{non}}$  is to macroscopically integrate latencies of all historical steps. Both kernels work together to

 $<sup>^6</sup>$ Grey dashlines in Figs. 4 to 7 represent the average strength of all  $T_h=4$  steps. It serves as a baseline when estimating latencies, like a past step can be considered delayed to take effect if its curve lies below this line initially.

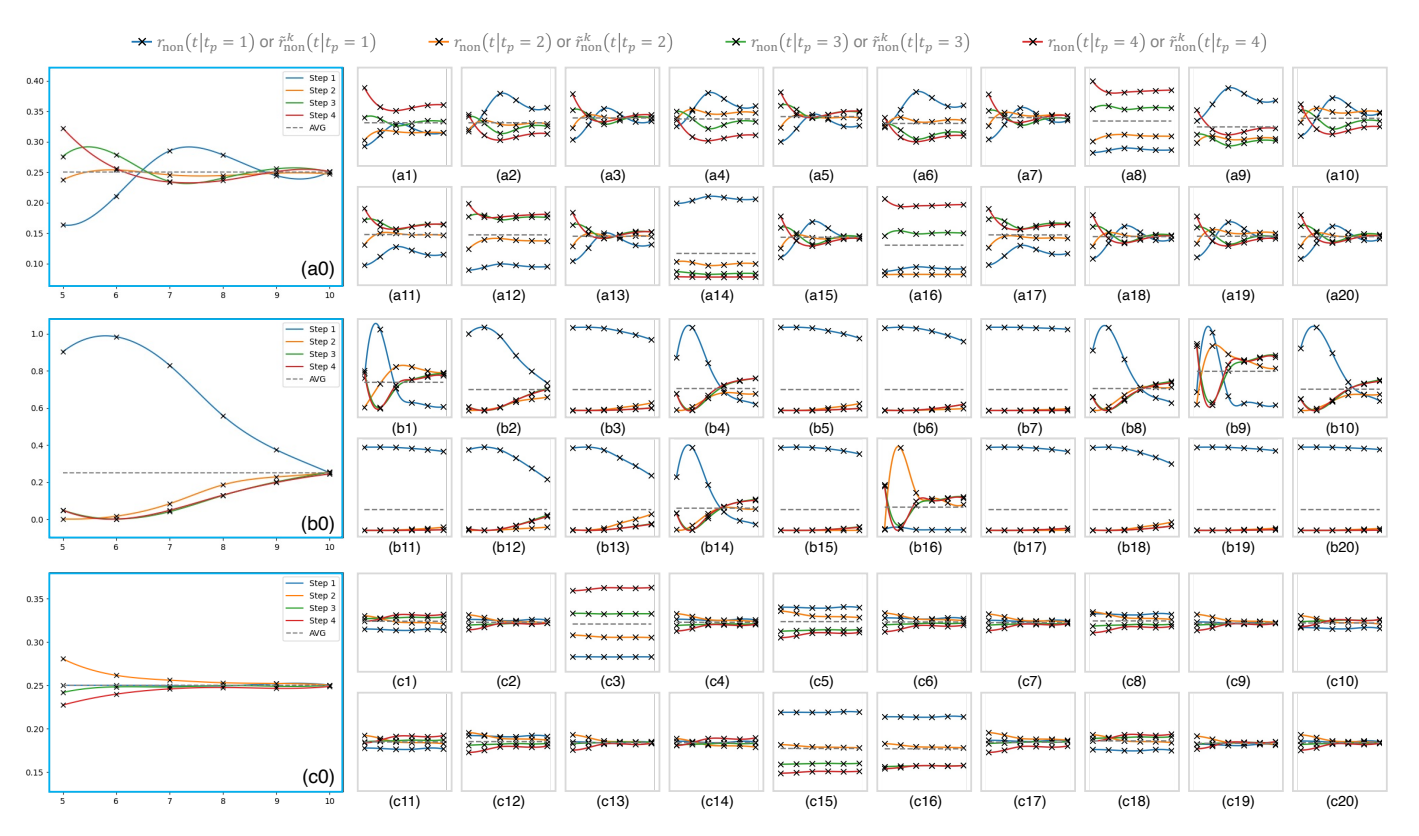


Fig. 5. Examples of the original non-interactive reverberation strength  $r_{\text{non}}(t|t_p)$  ( $t_p \in \{1, 2, 3, 4\}$ , in blue boxes) and its  $K_g = 20$  altered  $\tilde{r}_{\text{non}}^k(t|t_p)$  ( $t_p \in \{1, 2, 3, 4\}$ ,  $k \in \{1, 2, ..., K_g\}$ ) curves after applying the generating kernel  $\mathbf{G}_{\text{non}}$ . k refers to indices of subfigures in grey boxes.

achieve our goal of learning and forecasting unique latency preferences for different ego agents for forecasting trajectories.

3) Social Reverberation  $r_{\rm soc}$ : Similar to the above non-interactive latencies, the proposed Rev model employs a social reverberation kernel  $\mathbf{R}_{\rm soc}$  and a social generating kernel  $\mathbf{G}_{\rm non}$  to cooperatively handle latencies within social events. We first discuss the social reverberation kernel  $\mathbf{R}_{\rm soc}$  and its corresponding social reverberation strength (curve).

Following previous works [40], an angle-based social-interaction-modeling strategy has been used to spatially and temporally represent social interactions when forecasting. Compared to the above non-interactive kernel  $\mathbf{R}_{\text{non}}$ , kernel  $\mathbf{R}_{\text{soc}}$  has been expanded to learn social latencies of all  $N_{\theta}$  angle-based partitions simultaneously. In our experiments,  $\mathbf{R}_{\text{soc}}$  is a 2D matrix with  $T_h N_{\theta}$  rows and  $T_f$  columns, so that each social event could be uniquely located both spatially ( $N_{\theta}$  angle partitions) and temporally ( $T_h$  steps), and then be bridged to each future step. For the ease of presentation, we treat it as a 3D tensor of  $N_{\theta} \times T_h \times T_f$ , and use symbol  $\mathbf{R}_{\text{soc}}[n,p,q]$  to index each element. Like Eq. (21), for any social partition  $n \in \{1,2,...,N_{\theta}\}$ , at any past step  $t_p \in \{1,2,...,T_h\}$ , given variable  $t \in \{T_h+1,...,T_h+T_f\}$ , we have the *Social Reverberation Strength* 

$$r_{\text{soc}}(t|n, t_p) = \frac{(\mathbf{R}_{\text{soc}}[n, t_p, t])^2}{\sum_{t_x=1}^{T_h} (\mathbf{R}_{\text{soc}}[n, t_x, t])^2}.$$
 (23)

Fig. 6 visualizes several social reverberation curves. It can be seen that different latencies have been predicted for

handling social events at different temporal steps and spatial positions. For example, in Fig. 6 (a0), the ego pedestrian is walking along with its companion, which is located in the 6th social partition relative to the ego one, with other neighbors far away from them spatially. In this case, we can regard that the main social trajectory-changing event for the ego pedestrian is to pay more attention to this companion and coordinate their future path together. Interestingly, predicted social reverberation curves in Fig. 6 (a6) - (a8) (bounded with blue boxes) present noticeably different latency preferences for handling these social events. In detail, subfigure (a0) shows that the neighbor pedestrian starts to increase its speed (relative to the ego one) at step 3 (5th and 6th observed frames), while before that step this pair of agents share almost the same speed for walking together. Correspondingly, such step 3 (the green curve) has been paid the most concentration at the most beginning of the prediction period in partitions 6 - 8 where this neighbor's trajectory and social behaviors were located. In addition, in these partitions, social events happened at step 2 have been delayed till the end of the prediction period, while the same step 2 has been consistently concerned for about 3 steps (2.4s, from step 2 to step 5) in other social partitions in Fig. 6 (a1) to (a5). Similar differences could be observed by comparing step 3 in Fig. 6 (c1) to (c3) and (c4) - (c8).

To further verify the sensitivity of this social reverberation kernel in distinguishing latencies of different social trajectory-changing events (*i.e.*, social interactions), as shown in Fig. 6 (b0) and (d0), we introduce the manual neighbor approach [41] to test how kernel  $\mathbf{R}_{\rm soc}$  responds to modify its latency

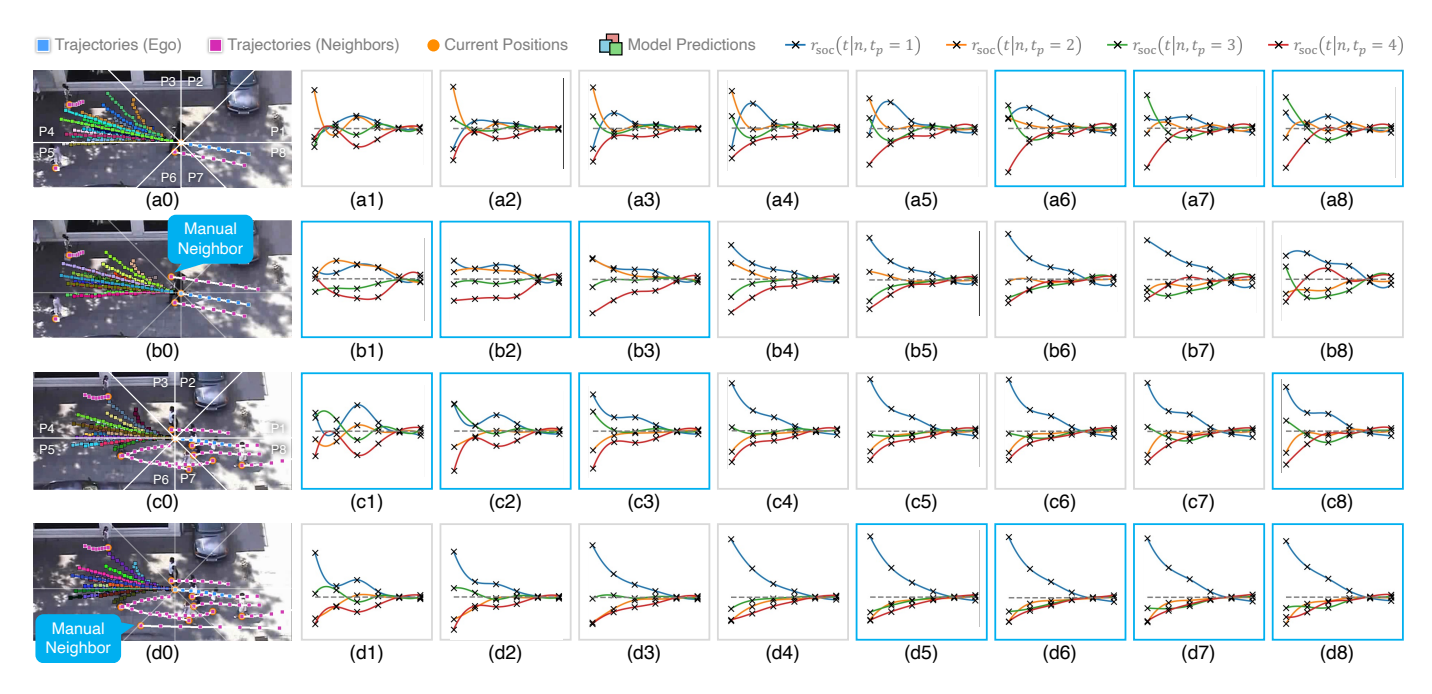


Fig. 6. Examples of social reverberation strength  $r_{soc}(t|n,t_p)$  for historical steps  $t_p \in \{1,2,3,4\}$  and social partition  $n \in \{1,2,...,8\}$ . Index of a subfigure in each row indicates the index of social partitions, like subfigure (a1) displays social reverberation strength in the partition 1. Cases (b0) and (d0) have been added manual neighbors [40] [41] upon the original (a0) and (c0) scenes to verify the sensitivity of reverberation curves to handle social interactions.

predictions for scenes where the social context has been intervened. For example, upon the original scene in Fig. 5 (a0), we have added a new companion to walk together with this ego pedestrian on its right-hand side, with a slightly higher but constant velocity. Compared to the original ones, social reverberation curves in the intervened social partitions (partitions 1 to 3, curves in Fig. 5 (b1) to (b3)) present significant differences in social latencies. In detail, in partition 2, social events that happened at step 4 have been suddenly delayed until step 9 to actually take effect, showing an overall social latency of about 5 steps (4.0s). Similar modifications of social latencies have been shown in Fig. 5 (d5) - (d8) after adding a new neighbor down to the ego agent in Fig. 5 (d0), where social events at step 1 have been forecasted to need more attention for the ego agent to handle while reducing the latencies of other social events that happened in these intervened partitions. These results could verify the sensitivity of the kernel  $\mathbf{R}_{\mathrm{soc}}$  for handling dynamics within social latencies under different interactive contexts when forecasting.

4) Altered Social Reverberation  $\tilde{r}_{\rm soc}$ : Similar to the above non-interactive discussions, social generating kernel  $\mathbf{G}_{\rm soc}$  alters social reverberation kernel  $\mathbf{R}_{\rm soc}$  in  $K_g$  ways to simulate randomness or multiple latency preferences for handling social interactions. Like Eq. (22), given a social partition n, the altered social reverberation strength (curve) is defined as

$$\tilde{r}_{\text{soc}}^{k}(t|n,t_{p}) = \frac{\left(\mathbf{R}_{\text{soc}}[n,t_{p},t] \ \mathbf{G}_{\text{soc}}[n,t_{p},k]\right)^{2}}{\sum_{t_{n}=1}^{T_{h}} \left(\mathbf{R}_{\text{soc}}[n,t_{x},t] \ \mathbf{G}_{\text{soc}}[n,t_{p},k]\right)^{2}}.$$
 (24)

For the ease of presentation, we select several specific social partitions in scenarios in Fig. 6 (a0) and (c0) to visualize how kernel  $\mathbf{G}_{\mathrm{soc}}$  alters the original reverberation curves. These results are reported in Fig. 7. Similar to discussions

in Sec. IV-D2, for a specific historical step  $t_p$  and a social partition n, it shows that  $\mathbf{G}_{\mathrm{soc}}$  still may not significantly change a single reverberation strength  $r_{\mathrm{soc}}(t|n,t_p)$  for any future step t, but provide alternatives for considering and accounting for social events from all steps and positions (social partitions) simultaneously. Notably, such alternatives are further associated with social events in their social partitions.

For example, in Fig. 7 (a0) - (a20), this partition 6 presents considerable unique latency preferences than other social partitions, as illustrated in Fig. 6 (a6). Under this situation, generating kernel  $G_{soc}$  recombines these four historical steps with a more "adventurous" attempt, like cases in Fig. 7 (a3) (a6) (a8) (a10) (a12) (a16) (a19) (a20), where the focus of all historical steps has been thoroughly rearranged compared to the original curve in Fig. 7 (a0). Similar results appear in Fig. 7 (c0) - (c20), corresponding to the social partition 1 in the original case in Fig. 6 (c0). As a comparison, for the social partition 1 in Fig. 7 (b0), which can be regarded as that almost no significant social trajectory-changing event has happened, more "conservative" alterations have been provided by the same generating kernel  $G_{\rm soc}$ . Among cases in Fig. 7 (b1) -(b20), only a few present noticeable rearrangements, like cases in (b2), (b6), (b16). Compared to the non-interactive  $G_{non}$ , this difference verifies that social interactions have become a main consideration, even for agents with different sociallatency-preferences, while the social generating kernel  $G_{\rm soc}$ has the ability to notice and learn this concern.

5) Latencies across Agents and Datasets: It can be seen from the above figures that latency curves (both non-interactive and social ones) may vary a lot for different agents for handling different historical steps or social interactions occurring in different locations. Fig. 8 visualizes the average of reverber-

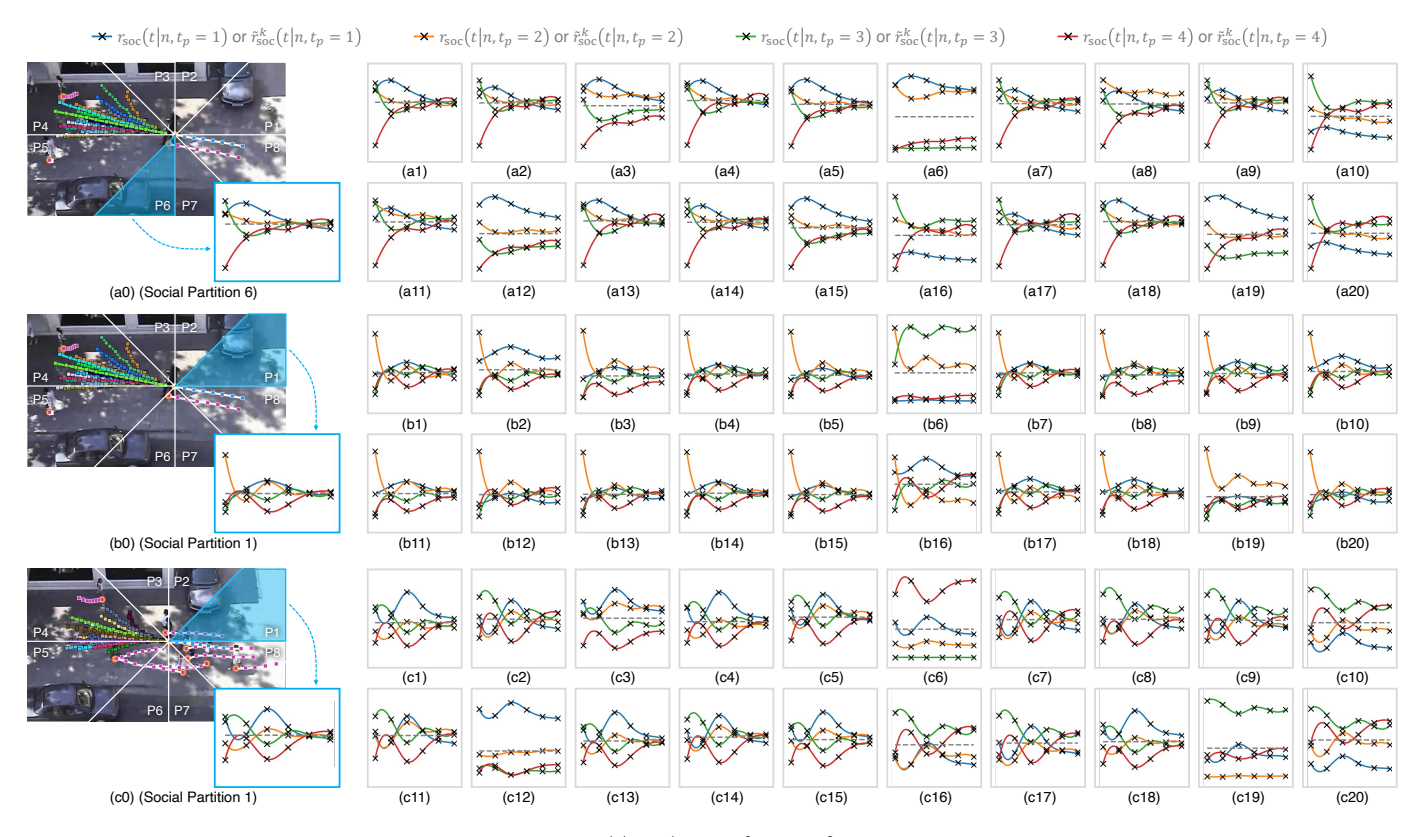


Fig. 7. Examples of the original social reverberation strength  $r_{\text{soc}}(t|n,t_p)$  ( $t_p \in \{1,2,3,4\}$ , given specific social partition n in blue boxes) and its  $K_g = 20$  altered  $\tilde{r}_{\text{soc}}^k(t|n,t_p)$  curves after applying the generating kernel  $\mathbf{G}_{\text{soc}}$ . k refers to indices of subfigures in grey boxes.

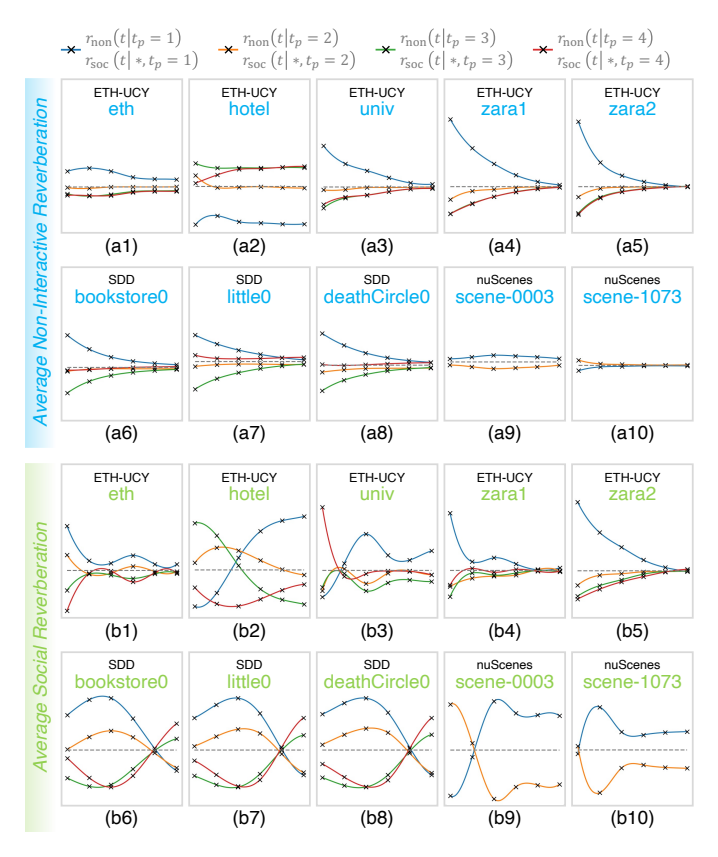


Fig. 8. Examples of average reverberation curves of all agents and all social partitions (only for social reverberation) on several datasets.  $\{T_h, T_f\}$  is set to  $\{4,6\}$  on ETH-UCY and SDD sets, while set to  $\{2,5\}$  on nuScenes.

ation curves on several datasets, representing agents' average latency preferences on these datasets<sup>7</sup> correspondingly.

For non-interactive cases, we observe that the first historical step 1 might be the first step to be concentrated on most sets. Like in Fig. 8 (a3) - (a8), the average curve shows that agents are forecasted to take at least a latency of 4 more steps (3.2s) to finish handling self-sourced trajectory-changing events that happened on the first observation step. This can be interpreted as that most agents may keep their motion status as those they presented from the beginning, meaning that such status may be remained for about 8 steps (6.4s) since step 1. During this period, the following steps may gradually be considered when planning trajectories. Curves of several other datasets like Fig. 8 (a2) (a9) (a10) show a different trend that almost all historical steps are considered equally contributed. We can infer that agents in these scenes may prefer to maintain their motion status all the time, like walking or driving alongside or around straight lines. Therefore, their latencies for handling non-interactive trajectory-changing events could be considered as 0, i.e., taking effect immediately.

Latencies for handling social trajectory-changing events present more diverse changes across datasets. For example, in Fig. 8, it predicts most agents may first handle events on the step 3 in the near future (last for about 2 steps / 1.6s), during which the historical step 1 has been delayed. This step 1 will be finally started to be handled by agents at step 8, long after 7 steps (5.6s) since occurrence. Differently, in SDD cases

<sup>&</sup>lt;sup>7</sup>See further discussions on latencies of motion prediction in Appendix C.

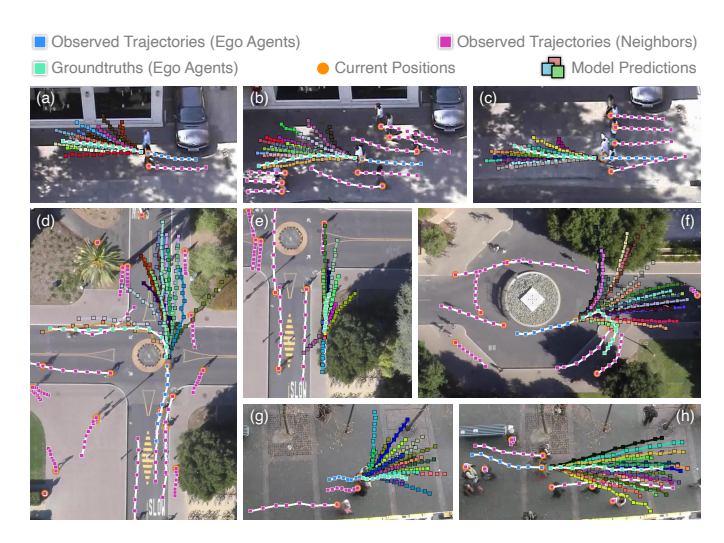


Fig. 9. Examples of visualized Rev predictions (20 generations).

in Fig. 8 (b6) - (b8), it predicts agents to firstly handle social events on steps 1 and 2 until step 7, while events on steps 3 and 4 are delayed for about 4 - 5 steps (3.2 - 4.0s) to be handled since their happening. Compared to the average non-interactive curves that present similar latency trends across datasets, such varying social curves could verify the dynamic-modeling capability of the proposed *Rev* for modeling agents' varying latency preferences for handling social events.

Also, it should be noted that nuScenes curves in Fig. 8 (a9) (a10) (b9) (b10) are obtained by only considering 2 historical steps for the future 5 steps. These curves indicate that distinguishing latency preferences could still be learned, even though they have extremely limited observations for the vehicle dataset nuScenes, highlighting the robustness of the proposed latency modeling approach and its possible applications in intelligent transportation systems.

6) Summary of Latencies: The proposed reverberation transform include two trainable while complementary kernels. The reverberation kernel **R** captures event-level latencies, typically exhibiting single-peaked curves that intuitively reflect the time to perceive, respond to, and complete trajectory-changing events, thereby enhancing the interpretability of how agents handles these events during planning. The generating kernel **G** encodes agents' global latency preferences and randomness, offering alternative arrangements of multiple events without altering specific latency curves. By combining these kernels together, the reverberation transform enables the Rev model to adaptively characterize and forecast heterogeneous and dynamic latency preferences when forecasting trajectories.

#### E. Further Discussions

Next, we further discuss how *Rev* model works when forecasting, from the modeling of social interactions, generalizability, and long-term prediction three aspects<sup>9</sup>.

ZARA1, USING "mV-n" TO DENOTE RESULTS UNDER best-of-n FOR MODELS TRAINED WITH m GENERATIONS DURING TRAINING.

$K_g$	$K_g$ V-10	$K_g$ V-20	$K_g$ V-40
1	0.401/0.851	0.397/0.839	0.393/0.828
2	0.331/0.677	0.327/0.667	0.324/0.658
5	0.253/0.491	0.246/0.474	0.240/0.458
10	0.211/0.390	0.206/0.377	0.202/0.364
20	0.242/0.466	0.172/0.283	0.167/0.272
30	0.247/0.473	0.191/0.334	0.163/0.263
40	0.252/0.493	0.192/0.339	0.146/0.219
	1 2 5 10 20 30	1 0.401/0.851 2 0.331/0.677 5 0.253/0.491 10 0.211/0.390 20 0.242/0.466 30 0.247/0.473	1 0.401/0.851 0.397/0.839 2 0.331/0.677 0.327/0.667 5 0.253/0.491 0.246/0.474 10 0.211/0.390 0.206/0.377 20 0.242/0.466 0.172/0.283 30 0.247/0.473 0.191/0.334

1) Social Interactions: Fig. 9 visualizes several Rev predictions. It can be seen that social interactions have been considered in the forecasted trajectories. For example, in Fig. 9 (a), the randomness of forecasted trajectories mainly lies on the right-hand side of the ego pedestrian, since there is a walking-together companion on the other side. In Fig. 9 (b), most forecasted trajectories have been bent to avoid the upcoming pedestrian group. Also, distinct turn choices have been forecasted in roundabout scenes in Fig. 9 (d) and (f), verifying its generalizability in complex scenes. Though some predictions may be considered as not suitable for the context, like crossing the border of roads in (d) and (f), such predictions could still prove the potential of the proposed Rev model in forecasting trajectories with only egos' and neighbors' observed trajectories, without the dependency on additional information like segmentation images or language models.

2) Generalizability: In the proposed Rev model, generating kernel G provides multiple latency preferences for the same ego agents to make decisions upon different trajectory-changing events, simulating stochastic properties in their future trajectories. We now further discuss its generalizability, taking MSN [6] as the baseline.

We first discuss the kernel shape  $(K_g)$ . It decides the number of trajectories generated during training. Like the symbols used in S-GAN [14], we use "nV-m" to denote the trainingtest configuration that generates n trajectories during training and test models under the best-of-m validation. In Tab. VII, we see that the number of generations during training  $(K_g$  in Rev models) heavily affects how they perform. Especially, results indicate that, with symbol mV-n, Rev models could achieve better performance when m is slightly larger than n, applicable to both  $K_g$ V-10 and  $K_g$ V-20 cases. Such results could prove the learning capability of the generating kernel G during the model training while also revealing limitations in generating trajectories far beyond its capacity (like using a G with  $K_g = 1$  to generate 40 stochastic trajectories).

Now we further discuss how  $K_g$  affects Rev models' performance by fixing the number of generated trajectories during testing (let m=K in nV-m). Several Rev-MSN variations have been conducted to serve as baselines by replacing generating kernels  $\mathbf{G}$  with the MSN-like generating strategy [6]. Results in Fig. 10 indicate that the generalizability of kernel  $\mathbf{G}$  is worse than MSN when only predicting one trajectory for each agent. However, Rev models perform much better when generating more numbers of trajectories. For example,

<sup>&</sup>lt;sup>8</sup>See Sec. IV-E3 for validations under long-term prediction settings.

<sup>&</sup>lt;sup>9</sup>See Appendix B for the discussions of model efficiency.

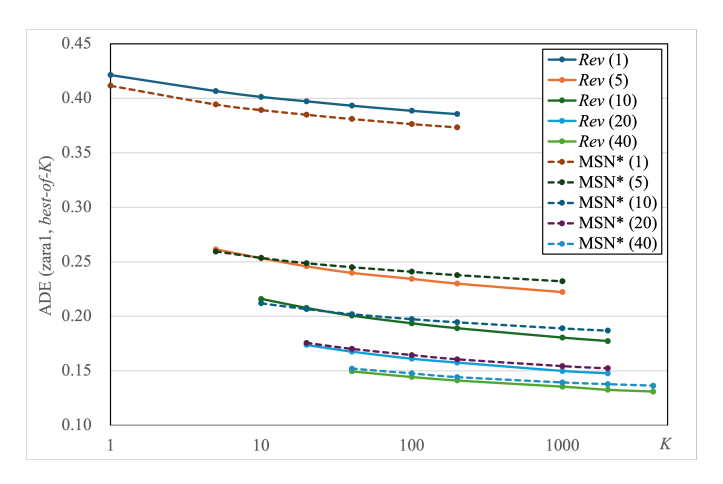


Fig. 10. Comparisons of generalizability ( $K_g$ V-K ADE on zara1) with MSN [6]. Numbers in brackets indicate  $K_g$  for Rev variations, and indicate the number of style channels for MSN variations.

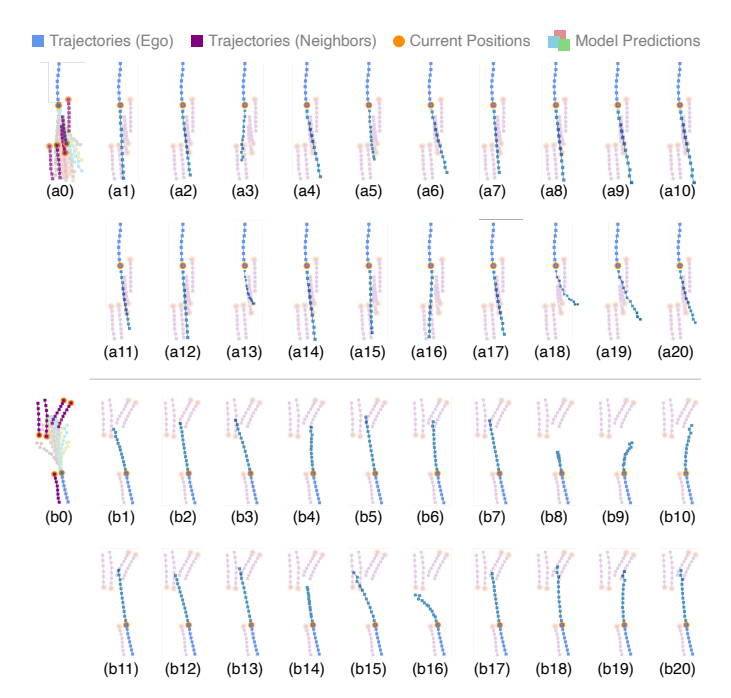


Fig. 11. Rev predictions under different latency combinations  $(K_g=20)$ . (a0) and (b0) include all predictions, while other subfigures are obtained through their corresponding kth column of generating kernels  $\mathbf{G} \in \mathbb{R}^{T_h \times K_g}$ .

 $Rev~(K_g=5)$  outperforms the corresponding MSN variation MSN\* (5) for about 4.28% ADE when generating K=1000 trajectories, while  $Rev~(K_g=10)$  even outperforms its MSN variation for about 5.12% when generating 2000 trajectories. Such results demonstrate the effectiveness of the kernel G in generating multiple latency preferences for handling trajectory-changing events, especially when more numbers of trajectories are needed to be forecasted.

To further verify our thoughts, Fig. 11 visualizes Rev predictions forecasted through different columns of generating kernels ( $K_g=20$ ). These predictions present unique preferences for handling interactive behaviors. For example, in case Fig. 11 (b0), the ego pedestrian is walking with a companion, with another duo of pedestrians approaching face-to-face. Though

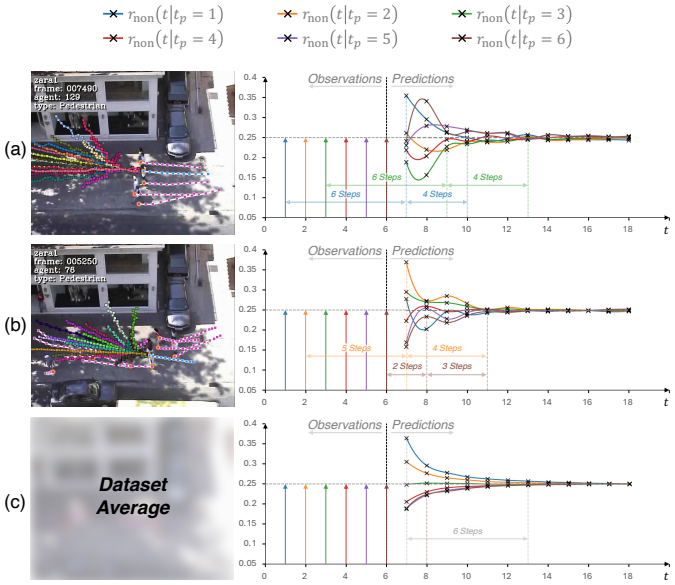


Fig. 12. Examples of non-interactive reverberation strength  $r_{\rm non}(t|t_p)$  under the long-term prediction setting  $\{T_h,T_f\}=\{6,12\}$   $(t_p\in\{1,2,3,4,5,6\})$ .

we have mentioned in the above discussions that kernel G may not significantly modify latency preferences of a single historical frame, subfigures (b1) - (b20) have presented quite different predictions *styles* [6], like keep walking and ignore the upcoming duo in (b1), slightly avoid them in (b4), notice and avoid them as quickly as possible in (b8) - (b10), and even head for them directly in (b16) - (b17). This implies that the way agents jointly consider the importance of historical events (frames) and selectively combine handle their latencies could lead to totally different future trajectory-choices, while the proposed generating kernels G have the ability to capture and learn such alternatives <sup>10</sup>, and finally generate interpretable while acceptable trajectories.

3) Latencies under Long-term Prediction Settings: Discussions in Secs. IV-D1 and IV-D3 indicate that pedestrians are forecasted having a latency for up to 6 - 8 frames (4.8 - 6.4s) to start handling a trajectory-changing event, during the whole  $T_h + T_f = 10$  steps (20 frames or 8.0s in total) of the prediction period. We now discuss whether such latency varies with the prediction period or remains a constant for specific prediction scenarios, taking the  $\{T_h, T_f\} = \{6, 12\}$  (36 frames or 14.4s in total) long-term setting as an example. In Fig. 12 (a) and (b), it can be seen that agents' latency preferences are still similar to the former curves we have discussed. For example, step 3 in case (a) has been delayed for about 6 steps (4.8s) to take effect at future step 9, and takes another 4 steps (3.2s) to keep concentrating on it, while similarly, step 2 in case (b) takes about 4 steps (3.2s) for the pedestrian to handle it since the first prediction step (step 7). We also visualize the average curve of this dataset in Fig. 12 (c), under this long-term setting. It shows that all historical events are predicted to be solved only after about 6 steps (4.8s) after the first prediction step, and then they will be paid almost the same concentration till

<sup>10</sup>This is actually associated with the low-rank properties of the proposed reverberation transform. See further discussions in Appendix A. the end of the prediction period, presenting similar trends as former short-term results shown in Fig. 8. We can conclude that such captured and forecasted latencies are associated with pedestrians' walking or social preferences, rather than the simple data-fitting, further providing insightful interpretations of pedestrian behaviors beyond trajectory prediction.

# V. CONCLUSION

In this manuscript, we proposed the Reverberation Transform and the corresponding Reverberation (short for Rev) trajectory prediction model to explicitly model and forecast agents' latencies for handling trajectory-changing events when forecasting trajectories. The proposed reverberation transform includes two trainable reverberation kernels, the reverberation kernel R characterizes event-level causal latencies while the generating kernel G simulates stochastic latency variations or randomness, providing a principled way to bridge agents' observations to the future while explicitly considering latencies for handling all trajectory-changing events. The proposed Rev model not only achieves competitive prediction accuracy across pedestrian and vehicle datasets (ETH-UCY, SDD, and nuScenes), but also demonstrates strong latencyinterpretability through the visualization of non-interactive and social reverberation curves. Ablation studies and discussions further verified the necessity of each component and the complementary effects of forecasting non-interactive and social latencies, highlighting the importance of explicitly modeling latency dynamics in trajectory prediction, offering new insights into how agents anticipate, react, and adapt to diverse trajectory-changing events.

Beyond the immediate gains in accuracy and interpretability, the proposed reverberation transform also provides a general theoretical perspective for quantifying latency dynamics in sequential decision-making. In future work, we plan to extend this framework to multi-modal perception inputs and more diverse spatio-temporal domains, such as human-robot interaction and autonomous driving. We believe that latency-aware forecasting will play a crucial role in improving both the safety and adaptability of intelligent systems.

#### REFERENCES

- A. Alahi, K. Goel, V. Ramanathan, A. Robicquet, L. Fei-Fei, and S. Savarese, "Social lstm: Human trajectory prediction in crowded spaces," in *Proceedings of the IEEE conference on computer vision and* pattern recognition, 2016, pp. 961–971. 1, 2, 3, 7
- [2] C. Zhang and C. Berger, "Pedestrian behavior prediction using deep learning methods for urban scenarios: A review," *IEEE Transactions on Intelligent Transportation Systems*, 2023.
- [3] J. Yue, D. Manocha, and H. Wang, "Human trajectory forecasting with explainable behavioral uncertainty," arXiv preprint arXiv:2307.01817, 2023.
- [4] Y. Zhang, W. Guo, J. Su, P. Lv, and M. Xu, "Bip-tree: Tree variant with behavioral intention perception for heterogeneous trajectory prediction," *IEEE Transactions on Intelligent Transportation Systems*, 2023.
- [5] M. Golchoubian, M. Ghafurian, K. Dautenhahn, and N. L. Azad, "Pedestrian trajectory prediction in pedestrian-vehicle mixed environments: A systematic review," *IEEE Transactions on Intelligent Transportation Systems*, 2023.
- [6] C. Wong, B. Xia, Q. Peng, W. Yuan, and X. You, "Msn: multi-style network for trajectory prediction," *IEEE Transactions on Intelligent Transportation Systems*, vol. 24, pp. 9751 – 9766, 2023. 1, 2, 4, 7, 8, 14, 15

- [7] X. Zhou, X. Chen, and J. Yang, "Edge-enhanced heterogeneous graph transformer with priority-based feature aggregation for multi-agent trajectory prediction," *IEEE Transactions on Intelligent Transportation* Systems, 2024. 1, 3
- [8] C. Wang, Y. Wang, M. Xu, and D. J. Crandall, "Stepwise goal-driven networks for trajectory prediction," *IEEE Robotics and Automation Letters*, vol. 7, no. 2, pp. 2716–2723, 2022.
- [9] D. Guo, T. Mordan, and A. Alahi, "Pedestrian stop and go forecasting with hybrid feature fusion," in *IEEE 39th International Conference on Robotics and Automation (ICRA 2022)*, no. CONF, 2022.
- [10] Z. Liu, L. He, L. Yuan, K. Lv, R. Zhong, and Y. Chen, "Stagp: Spatio-temporal adaptive graph pooling network for pedestrian trajectory prediction," *IEEE Robotics and Automation Letters*, 2023. 1, 2
- [11] W. Mao, M. Liu, M. Salzmann, and H. Li, "Learning trajectory dependencies for human motion prediction," in *Proceedings of the IEEE/CVF International Conference on Computer Vision*, 2019, pp. 9489–9497. 1, 20
- [12] Z. Pei, X. Qi, Y. Zhang, M. Ma, and Y.-H. Yang, "Human trajectory prediction in crowded scene using social-affinity long short-term memory," *Pattern Recognition*, vol. 93, pp. 273–282, 2019. [Online]. Available: https://www.sciencedirect.com/science/article/pii/S0031320319301712 1, 2
- [13] A. Jain, A. R. Zamir, S. Savarese, and A. Saxena, "Structural-rnn: Deep learning on spatio-temporal graphs," in *Proceedings of the ieee* conference on computer vision and pattern recognition, 2016, pp. 5308– 5317. 1, 3
- [14] A. Gupta, J. Johnson, L. Fei-Fei, S. Savarese, and A. Alahi, "Social gan: Socially acceptable trajectories with generative adversarial networks," in Proceedings of the IEEE Conference on Computer Vision and Pattern Recognition, 2018, pp. 2255–2264. 1, 7, 14
- [15] C. Yu, X. Ma, J. Ren, H. Zhao, and S. Yi, "Spatio-temporal graph transformer networks for pedestrian trajectory prediction," in *European Conference on Computer Vision*. Springer, 2020, pp. 507–523. 1, 3
- [16] F. Giuliari, I. Hasan, M. Cristani, and F. Galasso, "Transformer networks for trajectory forecasting," pp. 10 335–10 342, 2021. 1, 2
- [17] T. Gu, G. Chen, J. Li, C. Lin, Y. Rao, J. Zhou, and J. Lu, "Stochastic trajectory prediction via motion indeterminacy diffusion," in *Proceedings of* the IEEE/CVF Conference on Computer Vision and Pattern Recognition, 2022, pp. 17113–17122. 1, 3, 7, 8
- [18] W. Mao, C. Xu, Q. Zhu, S. Chen, and Y. Wang, "Leapfrog diffusion model for stochastic trajectory prediction," in *Proceedings of the IEEE/CVF Conference on Computer Vision and Pattern Recognition*, 2023, pp. 5517–5526.
- [19] I. Bae, J. Lee, and H.-G. Jeon, "Can language beat numerical regression? language-based multimodal trajectory prediction," in *Proceedings of the IEEE/CVF Conference on Computer Vision and Pattern Recognition*, 2024, pp. 753–766.
- [20] C. Wong, B. Xia, Z. Hong, Q. Peng, W. Yuan, Q. Cao, Y. Yang, and X. You, "View vertically: A hierarchical network for trajectory prediction via fourier spectrums," in *European Conference on Computer Vision*. Springer, 2022, pp. 682–700. 1, 20
- [21] C. Wong, Z. Zou, and B. Xia, "Resonance: Learning to predict social-aware pedestrian trajectories as co-vibrations," in *Proceedings of the IEEE/CVF International Conference on Computer Vision (ICCV)*, 2025. 1, 3, 5, 6, 7, 8, 9, 10, 22
- [22] C. W. Granger, "Investigating causal relations by econometric models and cross-spectral methods," *Econometrica: journal of the Econometric* Society, pp. 424–438, 1969.
- [23] D. R. Heise, Causal analysis. John Wiley & Sons, 1975. 2
- [24] D. Helbing and P. Molnar, "Social force model for pedestrian dynamics," Physical review E, vol. 51, no. 5, p. 4282, 1995. 2, 3
- [25] P. Fiorini and Z. Shiller, "Motion planning in dynamic environments using velocity obstacles," *The international journal of robotics research*, vol. 17, no. 7, pp. 760–772, 1998.
- [26] J. Van den Berg, M. Lin, and D. Manocha, "Reciprocal velocity obstacles for real-time multi-agent navigation," in 2008 IEEE international conference on robotics and automation. Ieee, 2008, pp. 1928–1935.
- [27] B. Kim, C. M. Kang, J. Kim, S. H. Lee, C. C. Chung, and J. W. Choi, "Probabilistic vehicle trajectory prediction over occupancy grid map via recurrent neural network," in 2017 IEEE 20th International Conference on Intelligent Transportation Systems (ITSC). IEEE, 2017, pp. 399–404. 2, 3
- [28] J. Sun, Q. Jiang, and C. Lu, "Recursive social behavior graph for trajectory prediction," in *Proceedings of the IEEE/CVF Conference on Computer Vision and Pattern Recognition*, 2020, pp. 660–669. 2, 3
- [29] P. Zhang, W. Ouyang, P. Zhang, J. Xue, and N. Zheng, "Sr-Istm: State refinement for 1stm towards pedestrian trajectory prediction," in

- Proceedings of the IEEE Conference on Computer Vision and Pattern Recognition, 2019, pp. 12085–12094. 2
- [30] P. Zhang, J. Xue, P. Zhang, N. Zheng, and W. Ouyang, "Social-aware pedestrian trajectory prediction via states refinement lstm," *IEEE transactions on pattern analysis and machine intelligence*, vol. 44, no. 5, pp. 2742–2759, 2022. 2
- [31] N. Deo and M. M. Trivedi, "Convolutional social pooling for vehicle trajectory prediction," in *Proceedings of the IEEE Conference on Com*puter Vision and Pattern Recognition Workshops, 2018, pp. 1468–1476.
- [32] A. Vemula, K. Muelling, and J. Oh, "Social attention: Modeling attention in human crowds," in 2018 IEEE international Conference on Robotics and Automation (ICRA). IEEE, 2018, pp. 1–7.
- [33] T. Fernando, S. Denman, S. Sridharan, and C. Fookes, "Soft+ hardwired attention: An 1stm framework for human trajectory prediction and abnormal event detection," *Neural networks*, vol. 108, pp. 466–478, 2018. 2
- [34] Y. Yuan, X. Weng, Y. Ou, and K. M. Kitani, "Agentformer: Agent-aware transformers for socio-temporal multi-agent forecasting," in *Proceedings* of the IEEE/CVF International Conference on Computer Vision (ICCV), 2021, pp. 9813–9823. 2, 7, 8
- [35] H. Zhao, W. Xu, M. Monfort, J. Choi, C. Baker, Y. Zhao, H. Wu, A. Torralba, J. B. Tenenbaum, and B. Wu, "Tnt: Target-driven trajectory prediction," in *Advances in Neural Information Processing Systems* (NeurIPS), 2020. 2
- [36] B. Ivanovic and M. Pavone, "The trajectron: Probabilistic multi-agent trajectory modeling with dynamic spatiotemporal graphs," in *Proceedings of the IEEE International Conference on Computer Vision*, 2019, pp. 2375–2384.
- [37] D. Cao, Y. Wang, J. Duan, C. Zhang, X. Zhu, C. Huang, Y. Tong, B. Xu, J. Bai, J. Tong et al., "Spectral temporal graph neural network for multivariate time-series forecasting," Advances in Neural Information Processing Systems, vol. 33, pp. 17766–17778, 2020.
- [38] A. Mohamed, K. Qian, M. Elhoseiny, and C. Claudel, "Social-stgcnn: A social spatio-temporal graph convolutional neural network for human trajectory prediction," in *Proceedings of the IEEE/CVF Conference on Computer Vision and Pattern Recognition*, 2020, pp. 14424–14432.
- [39] M. Li, S. Chen, Y. Zhao, Y. Zhang, Y. Wang, and Q. Tian, "Dynamic multiscale graph neural networks for 3d skeleton based human motion prediction," in *Proceedings of the IEEE/CVF conference on computer* vision and pattern recognition, 2020, pp. 214–223. 2
- [40] C. Wong, B. Xia, Z. Zou, Y. Wang, and X. You, "Socialcircle: Learning the angle-based social interaction representation for pedestrian trajectory prediction," in *Proceedings of the IEEE/CVF Conference on Computer Vision and Pattern Recognition*, 2024, pp. 19005–19015. 2, 7, 8, 11, 12, 22
- [41] C. Wong, B. Xia, Z. Zou, and X. You, "Socialcircle+: Learning the angle-based conditioned interaction representation for pedestrian trajectory prediction," arXiv preprint arXiv:2409.14984, 2024. 2, 6, 7, 8, 11, 12, 22
- [42] I. Bae, J. Lee, and H. G. Jeon, "Social reasoning-aware trajectory prediction via multimodal language model," *IEEE Transactions on Pattern Analysis and Machine Intelligence*, 2025, accepted/In press. 2, 3
- [43] I. Bae, J. Lee, and H.-G. Jeon, "Can language beat numerical regression? language-based multimodal trajectory prediction," in *Proceedings of the IEEE/CVF Conference on Computer Vision and Pattern Recognition* (CVPR), 2024. 2, 3
- [44] Z. Zou, C. Wong, B. Xia, and X. You, "Who walks with you matters: Perceiving social interactions with groups for pedestrian trajectory prediction," in *Proceedings of the IEEE/CVF International Conference* on Computer Vision Workshops, 2025. 3
- [45] J. Martinez, M. J. Black, and J. Romero, "On human motion prediction using recurrent neural networks," in *Proceedings of the IEEE conference* on computer vision and pattern recognition, 2017, pp. 2891–2900.
- [46] H. Xue, D. Q. Huynh, and M. Reynolds, "Ss-lstm: A hierarchical lstm model for pedestrian trajectory prediction," in 2018 IEEE Winter Conference on Applications of Computer Vision (WACV). IEEE, 2018, pp. 1186–1194.
- [47] H. Manh and G. Alaghband, "Scene-Istm: A model for human trajectory prediction," arXiv preprint arXiv:1808.04018, 2018.
- [48] N. Bisagno, B. Zhang, and N. Conci, "Group Istm: Group trajectory prediction in crowded scenarios," in *Proceedings of the European* conference on computer vision (ECCV) workshops, 2018, pp. 0–0. 3
- [49] J. Ngiam, B. Caine, V. Vasudevan, Z. Zhang, H.-T. L. Chiang, J. Ling, R. Roelofs, A. Bewley, C. Liu, A. Venugopal *et al.*, "Scene transformer:

- A unified architecture for predicting multiple agent trajectories," arXiv preprint arXiv:2106.08417, 2021. 3
- [50] Z. Zhou, L. Ye, J. Wang, K. Wu, and K. Lu, "Hivt: Hierarchical vector transformer for multi-agent motion prediction," in *Proceedings of the IEEE/CVF Conference on Computer Vision and Pattern Recognition*, 2022, pp. 8823–8833. 3
- [51] L. Shi, L. Wang, S. Zhou, and G. Hua, "Trajectory unified transformer for pedestrian trajectory prediction," in *Proceedings of the IEEE/CVF International Conference on Computer Vision*, 2023, pp. 9675–9684.
- [52] D. Rempe, Z. Luo, X. B. Peng, Y. Yuan, K. Kitani, K. Kreis, S. Fidler, and O. Litany, "Trace and pace: Controllable pedestrian animation via guided trajectory diffusion," arXiv preprint arXiv:2304.01893, 2023. 3
- [53] I. Bae, Y.-J. Park, and H.-G. Jeon, "Singulartrajectory: Universal trajectory predictor using diffusion model," arXiv preprint arXiv:2403.18452, 2024.
- [54] R. Li, C. Li, D. Ren, G. Chen, Y. Yuan, and G. Wang, "Bcdiff: Bidirectional consistent diffusion for instantaneous trajectory prediction," Advances in Neural Information Processing Systems, vol. 36, 2024.
- [55] Y. Choi, R. C. Mercurius, S. M. A. Shabestary, and A. Rasouli, "Dice: Diverse diffusion model with scoring for trajectory prediction," in 2024 IEEE Intelligent Vehicles Symposium (IV). IEEE, 2024, pp. 3023–3029.
  3. 7. 8
- [56] M. Krstic, "Delay compensation for nonlinear, adaptive, and pde systems," 2009. 3
- [57] P. Cortes, J. Rodriguez, C. Silva, and A. Flores, "Delay compensation in model predictive current control of a three-phase inverter," *IEEE Transactions on Industrial Electronics*, vol. 59, no. 2, pp. 1323–1325, 2011. 3
- [58] G. R. Grice, R. Nullmeyer, and V. A. Spiker, "Human reaction time: toward a general theory." *Journal of Experimental Psychology: General*, vol. 111, no. 1, p. 135, 1982. 3
- [59] M. F. Bradshaw and S. J. Watt, "A dissociation of perception and action in normal human observers: The effect of temporal-delay," *Neuropsychologia*, vol. 40, no. 11, pp. 1766–1778, 2002. 3
- [60] A. Vaswani, N. Shazeer, N. Parmar, J. Uszkoreit, L. Jones, A. N. Gomez, Ł. Kaiser, and I. Polosukhin, "Attention is all you need," in *Advances in neural information processing systems*, 2017, pp. 5998–6008.
- [61] S. Pellegrini, A. Ess, K. Schindler, and L. Van Gool, "You'll never walk alone: Modeling social behavior for multi-target tracking," in 2009 IEEE 12th International Conference on Computer Vision. IEEE, 2009, pp. 261–268. 7
- [62] A. Lerner, Y. Chrysanthou, and D. Lischinski, "Crowds by example," Computer Graphics Forum, vol. 26, no. 3, pp. 655–664, 2007.
- [63] A. Robicquet, A. Sadeghian, A. Alahi, and S. Savarese, "Learning social etiquette: Human trajectory understanding in crowded scenes," in *European conference on computer vision*. Springer, 2016, pp. 549– 565.
- [64] J. Liang, L. Jiang, and A. Hauptmann, "Simaug: Learning robust representations from simulation for trajectory prediction," in *Proceedings of the European conference on computer vision (ECCV)*, August 2020. 7
- [65] J. Liang, L. Jiang, K. Murphy, T. Yu, and A. Hauptmann, "The garden of forking paths: Towards multi-future trajectory prediction," in *Proceedings of the IEEE/CVF Conference on Computer Vision and Pattern Recognition*, 2020, pp. 10508–10518.
- [66] H. Caesar, V. Bankiti, A. H. Lang, S. Vora, V. E. Liong, Q. Xu, A. Krishnan, Y. Pan, G. Baldan, and O. Beijbom, "nuscenes: A multimodal dataset for autonomous driving," arXiv preprint arXiv:1903.11027, 2019.
- [67] S. Saadatnejad, Y. Z. Ju, and A. Alahi, "Pedestrian 3d bounding box prediction," arXiv preprint arXiv:2206.14195, 2022. 7
- [68] M. Lee, S. S. Sohn, S. Moon, S. Yoon, M. Kapadia, and V. Pavlovic, "Muse-vae: Multi-scale vae for environment-aware long term trajectory prediction," in *Proceedings of the IEEE/CVF Conference on Computer Vision and Pattern Recognition*, 2022, pp. 2221–2230. 7, 8
- [69] M. Meng, Z. Wu, T. Chen, X. Cai, X. Zhou, F. Yang, and D. Shen, "Forecasting human trajectory from scene history," Advances in Neural Information Processing Systems, vol. 35, pp. 24920–24933, 2022. 7, 8
- [70] Y. Dong, L. Wang, S. Zhou, G. Hua, and C. Sun, "Recurrent aligned network for generalized pedestrian trajectory prediction," arXiv preprint arXiv:2403.05810, 2024. 7, 8
- [71] P. S. Chib, A. Nath, P. Kabra, I. Gupta, and P. Singh, "Ms-tip: Imputation aware pedestrian trajectory prediction," in *International Conference on Machine Learning*. PMLR, 2024, pp. 8389–8402. 7, 8
- [72] F. Marchetti, F. Becattini, L. Seidenari, and A. Del Bimbo, "Smemo: social memory for trajectory forecasting," *IEEE Transactions on Pattern Analysis and Machine Intelligence*, 2024. 7, 8

- [73] P. S. Chib and P. Singh, "Lg-traj: Llm guided pedestrian trajectory prediction," arXiv preprint arXiv:2403.08032, 2024. 7, 8
- [74] Y. Wu, L. Wang, S. Zhou, J. Duan, G. Hua, and W. Tang, "Multi-stream representation learning for pedestrian trajectory prediction," in *Proceedings of the AAAI Conference on Artificial Intelligence*, vol. 37, no. 3, 2023, pp. 2875–2882. 7, 8
- [75] X. Lin, T. Liang, J. Lai, and J.-F. Hu, "Progressive pretext task learning for human trajectory prediction," in *European Conference on Computer Vision*. Springer, 2024, pp. 197–214. 7, 8
- [76] B. Xia, C. Wong, D. Xu, Q. Peng, and X. You, "Another vertical view: A hierarchical network for heterogeneous trajectory prediction via spectrums," *IEEE Transactions on Pattern Analysis and Machine Intelligence*, 2025. 7, 8, 10, 20
- [77] K. Mangalam, Y. An, H. Girase, and J. Malik, "From goals, waypoints & paths to long term human trajectory forecasting," in *Proceedings of the IEEE/CVF International Conference on Computer Vision*, 2021, pp. 15 233–15 242. 7, 8
- [78] Y. Liu, Z. Ye, R. Wang, B. Li, Q. Z. Sheng, and L. Yao, "Uncertainty-aware pedestrian trajectory prediction via distributional diffusion," Knowledge-Based Systems, p. 111862, 2024. 7, 8
- [79] T. Maeda and N. Ukita, "Fast inference and update of probabilistic density estimation on trajectory prediction," in *Proceedings of the IEEE/CVF International Conference on Computer Vision*, 2023, pp. 9795–9805. 7, 8
- [80] L. Shi, L. Wang, C. Long, S. Zhou, W. Tang, N. Zheng, and G. Hua, "Representing multimodal behaviors with mean location for pedestrian trajectory prediction," *IEEE Transactions on Pattern Analysis and Ma*chine Intelligence, 2023. 7, 8
- [81] D. Cao, J. Li, H. Ma, and M. Tomizuka, "Spectral temporal graph neural network for trajectory prediction," in 2021 IEEE International Conference on Robotics and Automation (ICRA). IEEE, 2021, pp. 1839–1845. 7, 8
- [82] Y. Su, Y. Li, W. Wang, J. Zhou, and X. Li, "A unified environmental network for pedestrian trajectory prediction," in *Proceedings of the AAAI Conference on Artificial Intelligence*, vol. 38, no. 5, 2024, pp. 4970– 4978. 7, 8
- [83] T. Salzmann, B. Ivanovic, P. Chakravarty, and M. Pavone, "Trajectron++: Dynamically-feasible trajectory forecasting with heterogeneous data," in Proceedings of the European conference on computer vision (ECCV). Springer, 2020, pp. 683–700. 7, 8
- [84] H. Yang, Y. Tian, C. Tian, H. Yu, W. Lu, C. Deng, and X. Sun, "Sopermodel: Leveraging social perception for multi-agent trajectory prediction," *IEEE Transactions on Geoscience and Remote Sensing*, 2025. 7, 8
- [85] Y. Xu and Y. Fu, "Adapting to length shift: Flexilength network for trajectory prediction," in Proceedings of the IEEE/CVF Conference on Computer Vision and Pattern Recognition, 2024, pp. 15226–15237. 7,
- [86] C. Ionescu, D. Papava, V. Olaru, and C. Sminchisescu, "Human3. 6m: Large scale datasets and predictive methods for 3d human sensing in natural environments," *IEEE transactions on pattern analysis and machine intelligence*, vol. 36, no. 7, pp. 1325–1339, 2013. 20
- [87] C. S. Catalin Ionescu, Fuxin Li, "Latent structured models for human pose estimation," in *International Conference on Computer Vision*, 2011.
- [88] C. Xu, R. T. Tan, Y. Tan, S. Chen, Y. G. Wang, X. Wang, and Y. Wang, "Eqmotion: Equivariant multi-agent motion prediction with invariant interaction reasoning," in *Proceedings of the IEEE/CVF Conference on Computer Vision and Pattern Recognition*, 2023, pp. 1410–1420. 20
- [89] L. Dang, Y. Nie, C. Long, Q. Zhang, and G. Li, "Msr-gcn: Multi-scale residual graph convolution networks for human motion prediction," in Proceedings of the IEEE/CVF International Conference on Computer Vision, 2021, pp. 11 467–11 476. 20
- [90] T. Ma, Y. Nie, C. Long, Q. Zhang, and G. Li, "Progressively generating better initial guesses towards next stages for high-quality human motion prediction," in *Proceedings of the IEEE/CVF Conference on Computer* Vision and Pattern Recognition, 2022, pp. 6437–6446. 20
- [91] M. Li, S. Chen, Z. Zhang, L. Xie, Q. Tian, and Y. Zhang, "Skeleton-parted graph scattering networks for 3d human motion prediction," in *European Conference on Computer Vision*. Springer, 2022, pp. 18–36.



Conghao Wong received the master's degree from Huazhong University of Science and Technology, Wuhan, in 2022, where he is currently pursuing the Ph.D. degree. His research interests include computer vision and pattern recognition.



**Ziqian Zou** received the master's degree from Huazhong University of Science and Technology, Wuhan, in 2025, where he is currently pursuing the Ph.D. degree. His research interests include pattern recognition and video understanding.



**Beihao Xia** received his Ph.D. degree in Huazhong University of Science and Technology, Wuhan, China, in 2023. His research interests include trajectory prediction, behavior analysis, and understanding.



Xinge You (Senior Member, IEEE) is currently a Professor in Huazhong University of Science and Technology. He received his Ph.D. degree from the Department of Computer Science, Hong Kong Baptist University in 2004. His research have expounded in 200+ publications, such as IEEE TPAMI, TIP, TNNLS, CVPR, ECCV, ICCV. He served/serves as an Associate Editor of the *IEEE TCyb*, *TSMCA*. His research interests include wavelet analysis, pattern recognition, machine learning, and computer vision.

#### APPENDIX A

# PROPERTIES OF REVERBERATION TRANSFORM

We now discuss potential theoretical properties of the proposed reverberation transform, providing insights into why it could model and forecast latencies.

1) Linear Property: For the sequential similarity  $\mathbf{F} \in \mathbb{R}^{T_h \times T_h \times D}$ , the reverberation transform is defined (for any feature dimension  $d \in \{1, 2, ..., D\}$ ) as

$$\overline{\mathbf{F}}_{::d} = \mathcal{R}_{(\mathbf{R},\mathbf{G})}[\mathbf{F}_{::d}] := \mathbf{G}^{\top} \mathbf{F}_{::d} \mathbf{R} \in \mathbb{R}^{K_g \times T_f}, \qquad (25)$$

where d = 1, 2, ..., D denotes any feature dimension. It means that this transform is a bilinear operator for the sequential similarity, which shares a similar form as Fourier transforms.

Eq. (25) is linear-additive for any input  $\mathbf{F}$ , meaning that for any inputs  $\mathbf{F}_1$  and  $\mathbf{F}_2$ , given real numbers  $\alpha$  and  $\beta$ , we have

$$(\overline{\alpha \mathbf{F}_{1} + \beta \mathbf{F}_{2}})_{::d} = \mathbf{G}^{\top} (\alpha \mathbf{F}_{1} + \beta \mathbf{F}_{2})_{::d} \mathbf{R}$$

$$= \alpha \mathbf{G}^{\top} (\mathbf{F}_{1})_{::d} \mathbf{R} + \beta \mathbf{G}^{\top} (\mathbf{F}_{2})_{::d} \mathbf{R}$$

$$= \alpha (\overline{\mathbf{F}_{1}})_{::d} + \beta (\overline{\mathbf{F}_{2}})_{::d}.$$
(26)

This linear property actually provides us support for linearly decomposing latencies into non-interactive and social portions in the proposed *Rev* model, also ensures the event-level decoupled latency prediction when forecasting trajectories. It makes such transform inline with human intuitions for separately handling multiple trajectory-changing events, *i.e.*, people tend to process independent events separately and then superpose their effects when planning trajectories or future behaviors.

2) Approximate Completeness: According to Eq. (25), kernels  $\bf R$  and  $\bf G$  span a subspace of agents' possible latency mappings. In detail,  $\bf R$  establishes biases of agents to schedule historical trajectory determinants in the future, while  $\bf G$  recombines such biases and provides  $K_g$  alternatives of latencies.

For any  $\mathbf{F}$  (actually  $\mathbf{F}_{::d}$ , omit subscripts for clarity), we have

$$\operatorname{Row}\left(\mathbf{G}^{\top}\mathbf{F}\mathbf{R}\right) \subseteq \operatorname{Row}\left(\mathbf{G}^{\top}\right),\tag{27}$$

$$\operatorname{Col}\left(\mathbf{G}^{\top}\mathbf{F}\mathbf{R}\right)\subseteq\operatorname{Col}\left(\mathbf{R}\right).$$
 (28)

Thus, the transformed  $\overline{\mathbf{F}}$  lies in a bi-factor subspace limited by the row space of  $\mathbf{G}^{\top}$  and the column space of  $\mathbf{R}$ . Since  $\mathrm{rank}(\mathbf{R}) \leq \min\{T_h, T_f\}$  and  $\mathrm{rank}(\mathbf{G}) \leq \min\{T_h, K_g\}$ , this subspace cannot exceed

$$rank(\mathbf{R})rank(\mathbf{G}) \le \min\{T_h, T_f\} \min\{T_h, K_g\}, \qquad (29)$$

unless  $\operatorname{rank}(\mathbf{R}) = T_f$  and  $\operatorname{rank}(\mathbf{G}) = K_g$ . Considering that  $T_f$  might be larger than  $T_h$  under current common trajectory prediction settings, and  $K_g$  could also be larger than  $T_h$  when forecasting, the reverberation transform cannot be considered strictly complete. Also, we use  $\tanh$  to bound both reverberation kernels. Such bounds do not change rank in the algebraic sense but act as effective regularizers, making it an approximate rather than exact representation of extreme mappings.

This rank limitation explains why the transform spans a rich but structured subspace of latency mappings: rich enough (when **R** and **G** have higher rank) to approximate the finite-complexity latency patterns in real-world scenes, and structured enough (row or column space constraints) to regularize learning while preserving interpretability.

In short, approximate completeness follows from the fact that the reverberation transform has the ability to represent any matrix in a large bi-factor subspace of dimension up to  $\operatorname{rank}(\mathbf{R})\operatorname{rank}(\mathbf{G})$ , which can be made sufficiently expressive by learning kernels  $\mathbf{R}$  and  $\mathbf{G}$  to be *almost* full-rank under the experimental  $K_g, T_f, T_h$  settings. Especially, this approximate completeness ensures that the proposed *Rev* model can capture heterogeneous latency patterns without resorting to excessively high-dimensional parameterizations.

3) Low-Rank & Compression: According to Eq. (25), for any feature dimension  $d \in \{1, 2, ..., D\}$ , the rank of each transformed slice  $\overline{\mathbf{F}}_{::d}$  is bounded by

$$\operatorname{rank}(\overline{\mathbf{F}}_{::d}) \leq \min \left\{ \operatorname{rank}(\mathbf{G}), \operatorname{rank}(\mathbf{F}_{::d}), \operatorname{rank}(\mathbf{R}) \right\}.$$
 (30)

Under current common trajectory prediction settings, variations  $T_h, T_f, K_g$  mostly satisfy

$$K_a > T_f \ge T_h. \tag{31}$$

Specifically, sometimes  $K_g$  may be greater than  $T_f$ . Therefore, Eq. (30) has become

$$\operatorname{rank}\left(\overline{\mathbf{F}}_{::d}\right) \le \min\left\{T_h, T_f\right\}. \tag{32}$$

This means that the rank of the transformed  $\overline{\mathbf{F}}$  is independent of the number of latency generations  $K_g$  in real-world applications of trajectory prediction. In other words, the effective information dimension of the transformed  $\overline{\mathbf{F}}$  remains bounded by both  $T_h$  and  $T_f$ , and mostly only by the  $T_h$  in practice, indicating a low-rank and compression property of the reverberation transform.

In detail, it compresses the original similarity representation **F** into a subspace of dimension at most  $T_h$ , and the  $K_q$  output reverberation alternatives are different recombinations within this same subspace. This design produces apparent redundancy when  $K_q \gg T_h$ , but the redundancy is intentional-enabling diverse candidate predictions while ensuring that all outputs are constrained to a structured low-dimensional manifold. The low-rank property also plays as an inherent regularizer, which prevents the network from overfitting, even when the  $K_q$  is very large. It also makes the storage and computation more efficient, since the reverberation transform can be factorized through only two kernels R and G without explicitly materializing the full  $K_g \times T_f \times D$  feature matrix. Thus, this low-rank/compression property could ensure the Rev to generate diverse latencies and final predictions, while keeping their stablizability especially in high-dimensional trajectory prediction scenes.

# APPENDIX B EFFICIENCY ANALYSES

Trajectory prediction is a time-sensitive task, as it may be required to handle rapidly changing scenes, such as downtown roads or highways, in a timely manner. This section discusses the time/memory consumption of the proposed *Rev* models.

TABLE VIII INFERENCE TIMES AND MEMORY USAGES OF  $\mathit{Rev}$  Models ( $t_h=8$ ,  $t_f=12$ , forecasting 20 trajectories for each ego, on Apple M1 Mac mini). Variation settings are the same as Tab. V.

Model	Parameters	ADE/FDE (zara1)	Batch Size	Time (ms)	Memory (MB)
Rev	3,156,220	0.172/0.283	1 100 1000	30 47 190	37.14 115.09 535.30
Rev-a6	$\begin{array}{c} 1,216,670 \\ \text{(w/o } \Delta \hat{\mathbf{Y}}_{\mathrm{non}}^{i}) \end{array}$	0.174/0.294	1 100 1000	17 31 159	10.08 78.03 395.99
Rev-a7	$2,079,710$ (w/o $\Delta \hat{\mathbf{Y}}_{\mathrm{soc}}^{i}$ )	0.176/0.297	1 100 1000	15 22 45	16.21 26.29 116.70

All these efficiency tests are conducted on an Apple Mac mini (M1, 8GB memory, 2020) to simulate low-power mobile environments, rather than high-performance GPU servers.

As reported in Tab. VIII, Rev models present competitive computation efficiency. The full model could forecast trajectories for up to about 5263 ego agents per second, with each agent having 20 stochastic trajectories predicted. Meanwhile, its memory usages are still acceptable<sup>11</sup>, even though there are two Transformer backbones used to compute latencies within non-interactive and social trajectory-changing events.

Notably, variations a6 and a7 show better efficiencies, forecasting up to about 22,222 agents per second with lower memory needed. Although these variations may sacrifice some performance (about 2%/5% worse ADE/FDE on zara1) as a compromise, they offer alternatives for prediction scenarios with higher efficiency requirements, like some intelligent transportation systems and in-vehicle driving systems with limited computation resources and power deliverance, demonstrating the efficiency of the proposed *Rev* models.

# APPENDIX C LATENCIES FOR MOTION PREDICTION

Both the reverberation transform and the *Rev* model are designed for the trajectory prediction task. In this section, we further discuss their generalizability for other sequence forecasting tasks, taking the motion prediction dataset **Human3.6M** [86], [87] (3D skeleton prediction) as an example.

#### A. Datasets, Settings, and Metrics

Human3.6M is a large-scale dataset with 3.6 million 3D human poses by 11 professional actors in 15 scenarios (such as discussion, smoking, taking photos, and talking on the phone). Each scene only contains one subject. Following some previous works [76], [88], we regard this task as a 3D point forecasting task, where each frame contains a human skeleton made up of 17 3D points, by observing  $t_h = 10$  frames of positions and forecasting the next  $t_f = 10$  frames of positions under the sample rate of 25 Hz ( $\Delta t = 0.04$ s). Following their settings, subjects {1, 6, 7, 8, 9} will be used for training,

TABLE IX

Comparisons to other recent baseline methods on Human3.6M dataset. Metrics are reported as the MPJPE at different prediction horizons, including 80/160/320/400 milliseconds.

Models	80ms	160ms	320ms	400ms
Traj-GCN [11]	26.1	52.3	63.5	63.5
MSR-GCN [89]	12.1	25.6	51.6	62.9
PGBIG [90]	10.3	22.7	47.4	58.5
SPGSN [91]	10.4	22.3	47.1	58.3
EqMotion [88]	9.1	20.1	43.7	55.0
V <sup>2</sup> -Net (Haar) [20]	8.7	19.7	45.5	59.5
E-V <sup>2</sup> -Net (Haar) [76]	9.0	19.6	44.4	57.8
Rev (Ours)	9.5	18.9	41.5	53.7

subject 11 for validating, and subject 5 for testing. Compared to our discussed trajectory prediction scenes, this setting brings far more data dimensions and complexities, making it more challenging to forecast such human motions in the form of skeletons.

When training on Human3.6M, feature dimension d has been extended to 512 to suit the larger trajectory dimensionality. All noise-samplings in the Rev model are disabled to ensure the deterministic skeleton prediction. Also, social-interaction-modeling networks are removed from the original model, meaning that only non-interactive latencies will be considered when forecasting motions under this setting. When training, the learning rate (Adam) is set to 2e-4, and the maximum training epochs is set to 200. Other settings are the same as mentioned in the main manuscript.

Following previous works, we use the Mean Per Joint Position Error (MPJPE) to measure prediction performance. It is the average  $\ell_2$  distance between each predicted joint and its groundtruth, at some specific prediction step. For our considered  $\{t_h,t_f,\Delta t\}=\{10,10,0.04\}$  settings, MPJPEs at the 2nd/4th/8th/10th prediction steps (80/160/320/400 milliseconds) will be reported and compared.

#### B. Quantitative Analyses

Tab. IX reports the motion prediction performance of the proposed Rev model and several recent baseline methods. It can be seen that notable performance gains have been achieved by the proposed Rev. Compared to the newly published  $E-V^2$ -Net, Rev obtains up to 7.1% lower MPJPE across all prediction horizons. Notably, both V<sup>2</sup>-Net and E-V<sup>2</sup>-Net report their results using the Haar transform, which directly shows the performance improvements brought by the two proposed reverberation kernels, since the same usage of Haar transform in Rev. Compared to another sota EqMotion, the proposed Rev outperforms it for about 2.4% lower MPJPE at 400ms. Note that such validation is only conducted to roughly verify the overall usefulness of the proposed Rev model for handling different sequence forecasting tasks. Therefore, only this wellapplied dataset and limited number of baselines have been used for comparison. Thus, we have omitted further quantitative analyses like detailed ablations and statistical verifications.

However, *Rev* performs not as well as other baselines like EqMotion and E-V<sup>2</sup>-Net at the relatively short prediction

<sup>&</sup>lt;sup>11</sup>Memory usages reported in Tab. VIII only include memories allocated by neural networks and variables, using the MPS-backend PyTorch environment.

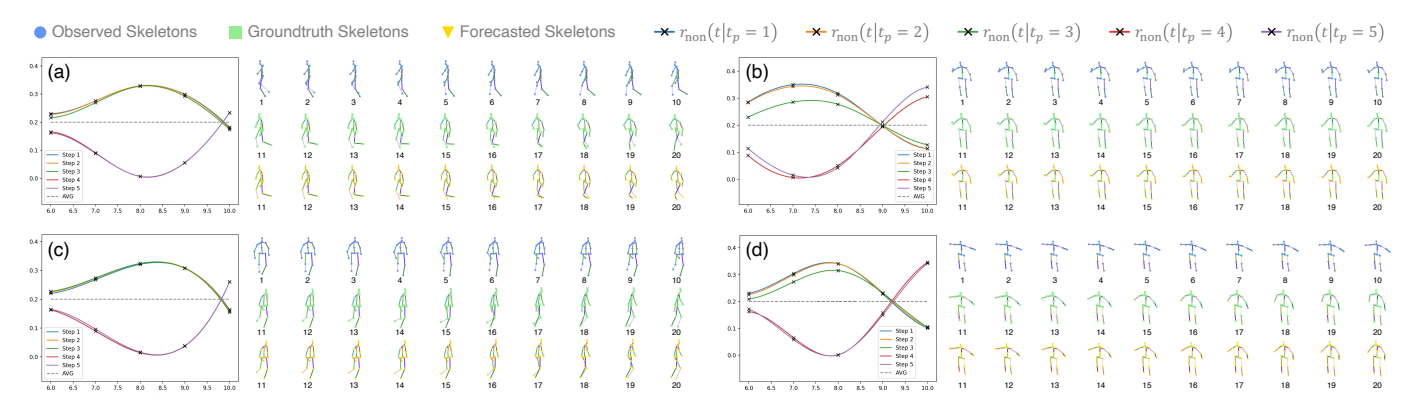


Fig. 13. Examples of non-interactive reverberation strength  $r_{\text{non}}(t|t_p)$   $(t_p \in 1, 2, 3, 4, 5)$  when forecasting human motions (3D skeletons,  $\{T_h, T_f\} = \{5, 5\}$ ).

horizon (MPJPE at 80ms, for about 5% worse). Interestingly, such performance drop aligns with the way how humans react to move their bodies physically, *i.e.*, there will always be latencies for changing their postures, meaning that those short-period motions may be challenging for the reverberation transform to model and forecast. Also, please note that only non-interactive latencies will be considered, meanwhile generating kernels **G** will degenerate into a set of constant values, since there are no human-human interactions and multigeneration needs under this motion-prediction-setting, leading to the limitations of model capabilities. Nevertheless, *Rev* still shows competitive performance for longer motion prediction periods, indicating the potential usefulness of the proposed reverberation transform and the *Rev* model beyond the only trajectory prediction task that it is specifically designed for.

# C. Discussions of Latencies within Motions

Similar to our discussions in the main manuscript, we now discuss how agents handle trajectory-changing events when planning their future motions in the form of 3D skeletons. For clarity, we still refer to words like motions or skeletons as *trajectories*. Since the removal of social-interaction-modeling networks and multiple generations in kernel  $\mathbf{G}$ , this section only discusses non-interactive latencies within human motions. Fig. 13 visualizes several non-interactive reverberation strengths computed from the non-interactive kernel  $\mathbf{R}_{\mathrm{non}}$ . Similar to our discussions in the main manuscript, 1 step in reverberation curves refers to 2 adjacent real-world frames (80ms per step) due to the use of Haar transform.

Focusing on Fig. 13 (a), it can be seen that this subject is observed running during the past 10 frames (5 steps), with its right leg moving forward (since frame 1 / step 1) while its left leg moving backward (since about frame 6 / step 3 or 4). Its groundtruth is inline with our intuition of running experiences that this subject may first keep its right leg still, then move its left leg forward after certain latencies of balancing its body (at about frame 15 / step 8 in the groundtruth). Such latency trends have been well captured and predicted by the kernel  $\mathbf{R}_{\mathrm{non}}$ , as illustrated by the reverberation curve in Fig. 13 (a). It predicts that the first 3 observation steps (frames 1 - 6) will be first concentrated and handled during steps 6 to 8,

corresponding to frames 11 - 16, which aligns with our "body-balancing" assumption. After that, the following 2 observation steps (frames 7 - 10) will be gradually taken into account in the further future, starting from step 8 - 9 (frames 15 - 18), thus presenting the trend of moving its left leg forward in the predictions. During this process, the latency of about 8 frames of body-balancing has been well captured and predicted.

Other examples in Fig. 13 also show unique latencies within human motions. In Fig. 13 (b), where the subject is finishing smoking and pushing the cigarette butt away, a latency of about 3 steps (6 frames) to shake off the ashes has been predicted, and the motion of putting its hand down has been well forecasted after such latency, starting from about step 8 (frame 16). Latencies of about 3 - 4 steps (6 - 8 frames) have also been captured in Fig. 13 (c) and (d) for forecasting different types of leg movements when running and lower arms from the Tpose then entering a relaxed state. Therefore, latencies within motions could still be learned and forecasted when forecasting, even though the proposed Rev is not specifically designed for this task while some of the model components have been disabled. Specifically, these latencies typically fall between 6 -8 frames (240ms - 320ms) across different actions, suggesting a consistent temporal delay in human motion responses, which these motion prediction baselines could hardly learn and explicitly forecast. Such results could verify the usefulness of reverberation transform and the Rev model for learning and handling latencies beyond the trajectory prediction task.

# APPENDIX D STATISTICAL VERIFICATIONS

Like most recent trajectory prediction approaches, the proposed *Rev* model could generate multiple random trajectories for each ego agent. Despite metrics like Negative Log-Likelihood (NLL) has been introduced to measure how the generated trajectory-distribution matches their original ones, most current approaches still can not better describe how well the diversities are of their multiple predicted trajectories. In addition, ADE and FDE are still the first choices of most researchers to measure their prediction performance. Therefore, this section further discuss the ADE/FDE of several recent baselines and the proposed *Rev* model, thus verifying potential statistical properties of these models straightforwardly.

 $0.2724 \pm 0.0137$ 

 $0.2145 \pm 0.0036$ 

 $0.1924 \pm 0.0021$ 

 $0.1730 \pm 0.0002$ 

 $0.1682 \pm 0.0001$ 

 $0.1656 \pm 0.0001$ 

 $0.1630 \pm 0.0001$ 

8

12

16 20

40

60

100

STAT	ISTICAI	L VERIFICATIONS OF	Rev MODEL ON ZAR.	A1. RESULTS ARE RE	EPORTED WITH "MEA	$\pm$ STD" COMPUTE	ED FROM 10 MODEL RUI
	$\overline{K}$	$minADE_K$	$meanADE_K$	$stdADE_K$	$minFDE_K$	$meanFDE_K$	$stdFDE_K$
	1	$0.7287 \pm 0.2243$	$0.7654 \pm 0.1903$	-	$1.6113 \pm 0.5291$	$1.6768 \pm 0.4327$	-
	2	$0.5354 \pm 0.1020$	$0.7541 \pm 0.0826$	$0.3704 \pm 0.0428$	$1.1541 \pm 0.2369$	$1.6528 \pm 0.2004$	$0.8522 \pm 0.1152$
	4	$0.3678 \pm 0.0483$	$0.7977 \pm 0.0341$	$0.4395 \pm 0.0475$	$0.7587 \pm 0.1081$	$1.7557 \pm 0.0771$	$1.0262 \pm 0.1230$

 $0.5330 \pm 0.0264$ 

 $0.3934 \pm 0.0090$ 

 $0.3343 \pm 0.0061$ 

 $0.2836 \pm 0.0009$ 

 $0.2693 \pm 0.0006$ 

 $0.2620 \pm 0.0001$ 

 $0.2544 \pm 0.0003$ 

 $0.4338 \pm 0.0354$ 

 $0.4201 \pm 0.0173$ 

 $0.4398 \pm 0.0048$ 

 $0.4348 \pm 0.0001$ 

 $0.4292 \pm 0.0001$ 

 $0.4275 \pm 0.0001$ 

 $0.4260 \pm 0.0001$ 

TABLE X STATISTICAL VERIFICATIONS OF *Rev* model on zara 1. Results are reported with "mean  $\pm$  std" computed from 10 model runs.

In the main manuscript, we refer to "minADE $_K$ /minFDE $_K$ " as "ADE/FDE". Differently, in this section, these metrics will be strictly distinguished, where "ADE/FDE" only indicates metrics computed from one generated trajectory, *i.e.*, the "minADE $_1$ /minFDE $_1$ ". We will report detailed results in the form of "meanADE $_K$   $\pm$  stdADE $_K$ " and "meanFDE $_K$   $\pm$  stdFDE $_K$ " to verify models' statistical performance. For ADE, these metrics are defined as

 $0.7666 \pm 0.0288$ 

 $0.7331 \pm 0.0279$ 

 $0.7577 \pm 0.0089$ 

 $0.7482\,\pm\,0.0002$ 

 $0.7481 \pm 0.0001$ 

 $0.7481 \pm 0.0001$ 

 $0.7481 \pm 0.0000$ 

meanADE<sub>K</sub> = 
$$\max_{k \in \{1, 2, \dots, K\}} \frac{1}{t_f} \sum_{t=t_h+1}^{t_h+t_f} \|\hat{\mathbf{p}}_{t_k}^i - \mathbf{p}_t^i\|_2$$
, (33)

$$stdADE_{K} = \underset{k \in \{1, 2, \dots, K\}}{std} \frac{1}{t_{f}} \sum_{t=t_{h}+1}^{t_{h}+t_{f}} \|\hat{\mathbf{p}}_{t_{k}}^{i} - \mathbf{p}_{t}^{i}\|_{2}.$$
 (34)

Similar computations are applied to compute meanFDE $_K$  and stdFDE $_K$ , based on the Eq. (20) in the main manuscript.

Take zara1 (a subset in ETH-UCY) as an example, Tab. X has reported several statistical ADE/FDE results, under different number of generations K. Note that all reported results are averaged over 10 runs to eliminate run-time randomness, therefore each single metric will be also reported in the form of "mean  $\pm$  std".

From Tab. X, we observe that the proposed Rev model exhibits stable and convergent statistical behaviors as the number of generations K increases. Specifically, both meanADE $_K$  and meanFDE $_K$  remain nearly constant when  $K \geq 8$ , with marginal variations smaller than 0.02, indicating that the overall distribution of generated trajectories is statistically stable even under multi-sample stochastic generation. Meanwhile, the minimum metrics (minADE $_K$ , minFDE $_K$ ) consistently decrease as K grows, verifying that the model can effectively produce multiple plausible trajectories and select more accurate ones when larger K values are available. This trend reflects a reasonable sampling diversity within the learned distribution rather than mere noise perturbation.

The standard deviations (stdADE<sub>K</sub>, stdFDE<sub>K</sub>) further quantify such diversity. When K increases from 2 to 12, stdADE<sub>K</sub> and stdFDE<sub>K</sub> gradually increase and then stabilize around 0.43 and 1.00, respectively. This indicates that the prediction spread among different generations is bounded and statistically consistent, suggesting that the diversity originates from meaningful variations in planning hypotheses rather than random fluctuations. Moreover, the extremely small deviations (on the order of  $10^{-4}$ ) for large K (e.g.,  $K \geq 20$ ) demonstrate

that the *Rev* model reaches an equilibrium sampling state where additional generations no longer change the statistical expectation of prediction performance.

 $1.6807 \pm 0.0678$ 

 $1.6067 \pm 0.0649$ 

 $1.6628 \pm 0.0195$ 

 $1.6413 \pm 0.0005$ 

 $1.6414 \pm 0.0001$ 

 $1.6414 \pm 0.0001$ 

 $1.6415 \pm 0.0001$ 

 $1.0086 \pm 0.0850$ 

 $0.9764 \pm 0.0420$ 

 $1.0228 \pm 0.0101$ 

 $1.0122 \pm 0.0005$ 

 $0.9993 \pm 0.0002$ 

 $0.9952 \pm 0.0001$ 

 $0.9918 \pm 0.0001$ 

Overall, these results confirm that the proposed reverberation-based formulation not only improves the best-case forecasting accuracy (minADE/minFDE) but also maintains a stable and interpretable trajectory distribution across multiple stochastic generations. The statistical convergence of ADE/FDE validates the robustness of the learned latency representations and the reliability of the *Rev* model under random sampling conditions.

#### AUTHOR'S NOTE

The opening quotations, "To live is to imagine ourselves in the future, and there we inevitably arrive." and "Though the future is a product of every present that precedes it, tomorrow does not belong to today." are adapted from Kobo Abe's In Search of the Present. They resonate with the theme of this manuscript: forecasting as a process of bridging past experiences and imagined futures.

This study continues the conceptual thread of our previous works SocialCircle [40], [41] and Resonance [21], but it is not a direct extension of either of these papers. Rather, it follows the same philosophical path that views trajectory prediction as a scan-reflect-echo process, which is a gradual experience from perception to resonance and then to reverberation. As illustrated in the first figure of Reverberation, forecasting trajectories can be interpreted as echolocation, i.e., scanning the surrounding space to perceive others. Resonance then emphasized how agents internally and socially reflect those perceived signals, aligning their spectrums through mutual responses. Building upon these ideas, Reverberation turns to the final stage, modeling how such reflections persist, decay, and re-emerge as temporal echoes across time, where finally the echolocation finished. Through this trilogy, the focus of our research evolves from where interactions happen (Reverberation), to how they co-vibrate across time (Resonance), and finally to when and for how long their influences live (Reverberation), pondering the question: how perception, causality, and anticipation are intertwined.